*The Canadian Mineralogist*
Vol. 43, pp. 263-294 (2005)

# REDISTRIBUTION OF THE RARE-EARTH ELEMENTS AMONG COEXISTING MINERALS IN METAMAFIC ROCKS ACROSS THE EPIDOTE-OUT ISOGRAD: AN EXAMPLE FROM THE ST. ANTHONY COMPLEX, NORTHERN NEWFOUNDLAND, CANADA

DANNY MULROONEY[§] AND TOBY RIVERS[¶]

*Department of Earth Sciences, Memorial University of Newfoundland, St. John's, Newfoundland A1B 3X5, Canada*

## ABSTRACT

Integrated results of *in situ* major-element and rare-earth-element analyses of coexisting Ca amphibole, plagioclase, epidote and titanite have been made from a suite of metamafic rocks from the St. Anthony Complex, Newfoundland, across the epidote-out reaction isograd to examine the redistribution of the REE as a consequence of the breakdown of epidote. Important major-element variations include a decrease in $X_{Cum}^{Amp}$ and an increase in $X_{An}^{Pl}$ across the reaction isograd, and an increase in $X_{Czo}^{Ep}$ within the epidote-amphibolite facies. These major-element changes correlate with variations in ΣREE and the LREE:HREE ratio in several of the phases, and also with systematic changes in $D^*_{REE}$ partitioning across the epidote-out isograd. Onuma-type diagrams for the partitioning of the REE between coexisting minerals confirm that the REE substitute at single elastic sites in titanite, epidote and plagioclase, whereas in Ca amphibole they occupy two sites, *M*4 and *M*4', with the size of the *M*4' peak being positively correlated with $X_{Cum}^{Amp}$ in Ca amphibole. A REE mass balance across the epidote-out isograd yields very good matches between the measured and reconstructed REE abundances in all cases, indicating that metamorphism was essentially isochemical with respect to the rare-earth elements, and that all the hosts for these elements were analyzed. The following major-element mass-balanced reaction, determined by the method of singular value decomposition from mineral compositions in representative samples of epidote amphibolite and plagioclase amphibolite from this ophiolitic complex, provides a realistic representation of the epidote-out isograd in the study area: $2.94\ CaAmp_1 + 5.00\ Pl_1 + 1.00\ Ep + 5.21Ttn_1 = 3.14\ CaAmp_2 + 5.65\ Pl_2 + 5.29\ Ttn_2$. Integration of the calculated stoichiometric coefficients of this reaction with the measured REE contents in each phase provides a good match for the MREE and HREE abundances, but a poorer match for the LREE, which show a deficiency on the product side. However, the results are compatible with the measured increases in LREE in Ca amphibole and plagioclase on the product side of the reaction, as a result of the breakdown of epidote and a reduction in LREE abundance in titanite. We highlight the role of epidote and titanite as the principal carriers of the REE in epidote amphibolite, and that of Ca amphibole as the dominant carrier in plagioclase amphibolite.

*Keywords*: rare-earth elements, Ca amphibole, plagioclase, epidote, titanite, LAM–ICP–MS data, distribution coefficient, crystal chemistry, mass balance, epidote-out isograd, St. Anthony Complex, Newfoundland.

## SOMMAIRE

Nous présentons les résultats intégrés d'analyses *in situ* pour les éléments majeurs et pour les terres rares des phases amphibole calcique, plagioclase, épidote and titanite d'une suite de roches métamafiques provenant du complexe de St. Anthony, à Terre-Neuve, de part et d'autre de la réaction isograde marquant la disparition de l'épidote, afin d'évaluer la redistribution des terres rares conséquente. Nous décelons des variation importantes, par exemple une diminution de $X_{Cum}^{Amp}$ et une augmentation de $X_{An}^{Pl}$ en traversant l'isograde, et une augmentation de $X_{Czo}^{Ep}$ dans les roches ayant atteint le faciès amphibolite à épidote. Ces changements impliquant les éléments majeurs sont accompagnés de variations en ΣREE et du rapport LREE:HREE dans plusieurs des minéraux, et aussi de changements systématiques du coefficient de partage $D^*_{REE}$. Des diagrammes dits de type Onuma exprimant la répartition des terres rares entre minéraux coexistants confirme que les terres rares sont incorporées à un seul site élastique dans la titanite, l'épidote et le plagioclase, tandis que dans l'amphibole calcique, elles occupent deux sites, *M*4 et *M*4', avec la dimension du pic pour *M*4' en correlation positive avec $X_{Cum}^{Amp}$. Un bilan de masses des terres rares en traversant l'isograde mène à une excellente correspondance entre les concentrations mesurées et reconstruites des terres rares dans tous les cas, indication que le métamorphisme était essentiellement isochimique par rapport aux terres rares, et que tous les minéraux hôtes de ces éléments ont été analysés. La réaction suivante, balancée par rapport aux masses des éléments majeurs et déterminée par la méthode de décomposition de valeurs singulières pour des compositions de minéraux dans des échantillons représentatifs d'amphibolite à épidote et d'amphibolite à plagioclase, représenterait de façon réaliste l'isograde marquant la disparition de l'épidote dans ce complexe ophiolitique: $2.94\ CaAmp_1 + 5.00\ Pl_1 + 1.00\ Ep + 5.21Ttn_1 = 3.14\ CaAmp_2 + 5.65\ Pl_2 + 5.29\ Ttn_2$.

*E-mail addresses*: [§]dmulrooney@hotmail.com, [¶] trivers@esd.mun.ca

L'intégration des coefficients stoechiométriques calculés de cette réaction avec les teneurs mesurées en terres rares dans chaque phase rend bien compte des abondances des terres rares moyennes et lourdes, mais nous trouvons une moins bonne correspondance pour les terres rares légères, qui sont déficitaires du côté des produits de la réaction. Toutefois, les résultats sont compatibles avec les augmentations mesurées des terres rares légères dans l'amphibole calcique et le plagioclase du côté des produits de réaction, comme conséquence de la déstabilisation de l'épidote et la réduction des abondances de terres rares légères dans la titanite. Nous soulignons le rôle de l'épidote et de la titanite comme hôtes principaux des terres rares dans l'amphibolite à épidote, et le rôle de l'amphibole calcique comme leur hôte principal dans l'amphibolite à plagioclase.

(Traduit par la Rédaction)

*Mots-clés*: terres rares, amphibole calcique, plagioclase, épidote, titanite, données LAM–ICP–MS, coefficient de distribution, cristallochimie, bilan des masses, isograde, disparition de l'épidote, complexe de St. Anthony, Terre Neuve.

## Introduction

Mineral parageneses in metamafic rocks are characterized by a limited number of phases with extensive solid-solutions, *e.g.*, chlorite, plagioclase, calcic amphibole, garnet, and calcic pyroxene. As a consequence, in low-variance assemblages, these minerals exhibit subtle changes in their major-element compositions as a function of changes in the whole-rock composition (*X*), modal abundance (*M*), and the pressure (*P*) and temperature (*T*) of metamorphism. These relationships have been qualitatively and quantitatively investigated for over 50 years, and the underlying principles are now broadly understood. As a result, for a given whole-rock composition, variations in the major-element mineral composition and mineral modes of the phases with changing *P* and *T* can now be modeled algebraically with reasonable precision (*e.g.*, Spear 1993).

The same cannot be said of trace-element mineral studies, however. Such investigations are in their infancy in metamorphic petrology. With the advent of microprobe instruments capable of measuring trace-element concentrations in individual mineral grains *in situ* at the ppm or even ppb level in small spots a few μm or tens of μm in diameter, *e.g.*, secondary ion mass spectrometer (SIMS), laser-ablation microprobe – inductively coupled plasma – mass spectrometer (LAM-ICP-MS), the tools to examine trace-element distributions within minerals are now available. With careful imaging prior to micro-analysis, problems with zoning and inclusions that plagued earlier trace-element studies of minerals can now be reduced or avoided; the *in situ* capability of the instrumentation allows the textural relationships with adjacent grains to be taken into account. Examples of modern trace-element mineral studies in metamorphic rocks, most of which have focussed on pelites, include those of Grauch (1989), Sorensen & Grossman (1989), Hickmott & Shimizu (1990), Hickmott & Spear (1992), Tribuzio *et al*. (1996), Bea *et al.* (1997), Nagasaki & Enami (1998), Yang *et al.* (1999), Pyle & Spear (1999, 2000), Yang & Rivers (2000, 2001, 2002), Zack *et al.* (2002), and Skublov & Drugova (2003). This study involves an investigation of the distribution of the rare-earth elements (REE) among the four phases, epidote, titanite, Ca amphibole and plagioclase, in a suite of amphibolite-facies metamafic rocks from the St. Anthony ophiolitic complex, in Newfoundland, across the epidote-out isograd. Epidote is a known carrier of the REE, especially the light REE (*e.g*., Pan & Fleet 1996). A general objective of the study thus is to establish the contents of the REE in coexisting minerals in epidote amphibolite and plagioclase amphibolite, its higher-grade equivalent above the epidote-out isograd. This objective is achieved through integrated major- and trace-element mineral analyses of all coexisting phases by electron-probe micro-analyzer (EPMA) and LAM–ICP–MS, respectively. These data permit the determination of partition coefficients for the light (L), middle (M), and heavy (H) REE amongst all pairs of coexisting minerals below and above the epidote-out isograd, and consequently allow an evaluation of the changes in REE partitioning as a result of the breakdown of epidote. Subsequently, using the combined major- and trace-element dataset for the minerals, we qualitatively evaluate structural and major-element compositional controls on the incorporation of REE in each of the four phases in order to determine possible site-distributions and substitution schemes. Abundances of the REE are then integrated with estimated modal proportions in a mass-balance study of rocks below and above the epidote-out isograd in order to evaluate the roles of individual phases as carriers of the REE in epidote amphibolite and plagioclase amphibolite, and to assess possible losses or gains of REE across the isograd. Finally, we use the method of singular value decomposition to calculate a mass-balanced model reaction for the epidote-out reaction isograd, and apply the calculated stoichiometric coefficients to the redistribution of REE across the isograd.

## Analytical Methods

### *Whole-rock analysis*

For eight samples, whole-rock concentrations of major elements were measured using a Fisons/ARL model 8420$^+$ sequential wavelength-dispersion X-ray spectrometer at the Department of Earth Sciences, Me-

morial University of Newfoundland. Samples were prepared as pressed pellets using a mixture of 5 grams of rock powder and 0.7 grams of BRP–5933 Bakelite® phenolic resin following the method of Longerich (1995). $FeO/Fe_2O_3$ was estimated by wet-chemical analysis following the method of Maxwell (1968).

Whole-rock concentrations of the fourteen REE were determined from solutions using a Hewlett Packard 4500$^+$ inductively coupled plasma – mass spectrometer (ICP–MS) at Memorial University of Newfoundland, following the $Na_2O_2$ sinter digestion procedure described by Longerich *et al.* (1996). Synthetic solutions were used to calibrate the instrument and standard reference solutions (MRG–1 and BR–688), and reagent blanks were analyzed for quality control.

*Electron imaging and micro-analysis*

Imaging and microanalysis were performed on thin sections 100 μm thick in order to provide sufficient thickness for LAM–ICP–MS analyses. Following standard optical petrography, selected samples were examined by back-scattered electron (BSE) imaging in order to assess individual grains for zoning, the presence of inclusions or alteration. For BSE imaging, standard operating conditions of a 10 nA beam current and 35 mm working distance were used. BSE images of potential micro-analysis sites, where phases appeared to be in textural equilibrium, were printed on a thermal wax printer to facilitate close spatial correlation between the locations of major- and trace-element analyses in subsequent analytical work. Quantitative major-element analyses were made on selected sites on the imaged grains in equilibrium assemblages using a Cameca SX–50 electron-probe micro-analyzer (EPMA) with a Link energy-dispersion (ED) detector at the Department of Earth Sciences, Memorial University of Newfoundland. An accelerating voltage of 10 to 20 kV, a beam current of 10 nA, and a beam diameter of 1 to 5 μm were used. The Link ED system was calibrated using a cobalt standard and the U.S. National Museum standard reference material 143965. Data reduction of raw counts was performed on-line using ZAF matrix-correction software.

Mineral trace-element concentrations were determined by LAM–ICP–MS at Memorial University of Newfoundland on the imaged grains previously analyzed by EPMA. Instrumentation and analytical procedures are described by Taylor *et al.* (1997) and Sylvester (2001). The instrument comprises a laser sampler utilizing a frequency-quadrupled Nd:YAG laser source with a 266 nm wavelength coupled to a Fisons VG PQII$^+$ "S" ICP–MS. The laser was operated in Q-switched mode with a pulse energy optically reduced to 0.5 mJ at a frequency of 10 Hz. Calibrations were made using the U.S. National Institute of Science and Technology (NIST) standard reference material (SRM) 612, a synthetic silicate glass, which has a "spiked" abundance of 50 ppm for 61 different elements (Pearce *et al.* 1997). Major-element concentrations, measured by EPMA, were used as internal standards (Ca for calcic amphibole, Si for epidote, titanite and plagioclase) to adjust for differences in ablation yield between samples and the calibration standard. Data acquisition was performed in peak-jumping mode with time-resolved analyses, and resulted in singular intensity data per mass peak. Typical acquisition-parameters were 60 to 80 seconds measurement of the argon carrier-gas blank, and 50 to 90 seconds measurement of the unknown with the laser switched on and material being ablated. Pit diameters varied from ~30 to 60 μm depending on the target material, pulse energy, and duration of ablation. The raw counts were processed off-line with CONVERT software, and data reduction was performed using LAMTRACE software (Jackson 2001). Since LAM–ICP–MS is a destructive *in situ* technique, it is impossible to perform repeated measurements on the same spot, thereby rendering it difficult to measure precision. To circumvent this problem, repeated analyses of U.S. Geological Survey glass reference BCR–2G have been performed under similar operating parameters to routine analyses, and in turn, are used to estimate precision. The analytical precision for all elements determined is within approximately 10% RSD (Appendix 1; Longerich 1996).

Potential sources of error are similar to those reported by Yang *et al.* (1999) and Yang & Rivers (2000). These include: (i) the different sizes of the electron and laser beams (μm for EPMA compared to tens of μm for LAM–ICP–MS), which can reduce accuracy if the normalizing elements for LAM–ICP–MS analyses (determined by EPMA) exhibit significant zoning at this scale, and (ii) fractionation in LAM–ICP–MS analysis during sample ablation and transportation to the mass spectrometer. To reduce the latter, the laser was defocused approximately 100–200 μm above the sample in this study.

## Modal Analysis

The extreme range in size of minerals in the samples (*i.e.*, tens of μm for titanite *versus* tens of mm for amphibole) rendered point counting impractical, so modal analyses were carried out using the program MODAN (Paktunc 1998), and verified by visual estimates. Input data for MODAN are the bulk-rock composition and the major-element compositions of all the phases. Uncertainties on the modes have not been calculated, but are likely small, although they may be significant for REE-rich phases such as titanite and epidote, as discussed later. On account of its low modal abundance and importance as a REE carrier, estimates of the modal abundance of titanite were refined using bulk-rock $TiO_2$ concentrations after first subtracting $TiO_2$ in other phases (principally the calcic amphibole).

## Samples and Petrography

This study involves eight samples of metabasic rocks from the inverted metamorphic gradient below the ophiolitic upper nappe known as the St. Anthony Complex in the Taconic Hare Bay Allochthon of western Newfoundland. Current understanding of the geological context of the Taconic allochthons in the Appalachians of western Newfoundland is summarized by Williams (1975, 1995). Details of the metamorphic field-gradient, mineral composition, and petrology of the metabasic assemblages in the metamorphic sole beneath the St. Anthony Complex are described by Jamieson (1979, 1981, 1986), who interpreted it as an amphibolite-facies shear zone formed between cold subducting continental-margin rocks and hot overriding oceanic lithosphere (Fig. 1). Our samples come from metabasic units known as the Goose Cove Schist and Green Ridge Amphibolite that, on the basis of their compositional similarity with less-deformed volcanic rocks in the footwall below the shear zone, are assumed to have been derived from them (Jamieson 1979, 1981). The structurally lowest parts of the Goose Cove Schist are spotted and banded greenschists composed of the assemblage chlorite – Ca amphibole (actinolite) – epidote – plagioclase – quartz (Fig. 1). However, these rocks are too fine-grained for analysis by LAM–ICP–MS; as a result, the sample suite is characterized by the following two assemblages: (i) Ca amphibole – epidote – plagioclase – titanite – quartz (epidote amphibolite), and (ii) Ca amphibole – plagioclase – titanite – quartz (plagioclase amphibolite).

In the *epidote amphibolite* (Fig. 2a), the Ca amphibole ("hornblende" on the basis of its olive green to brown pleochroic scheme) is the most abundant phase. It commonly contains inclusions of quartz and titanite.

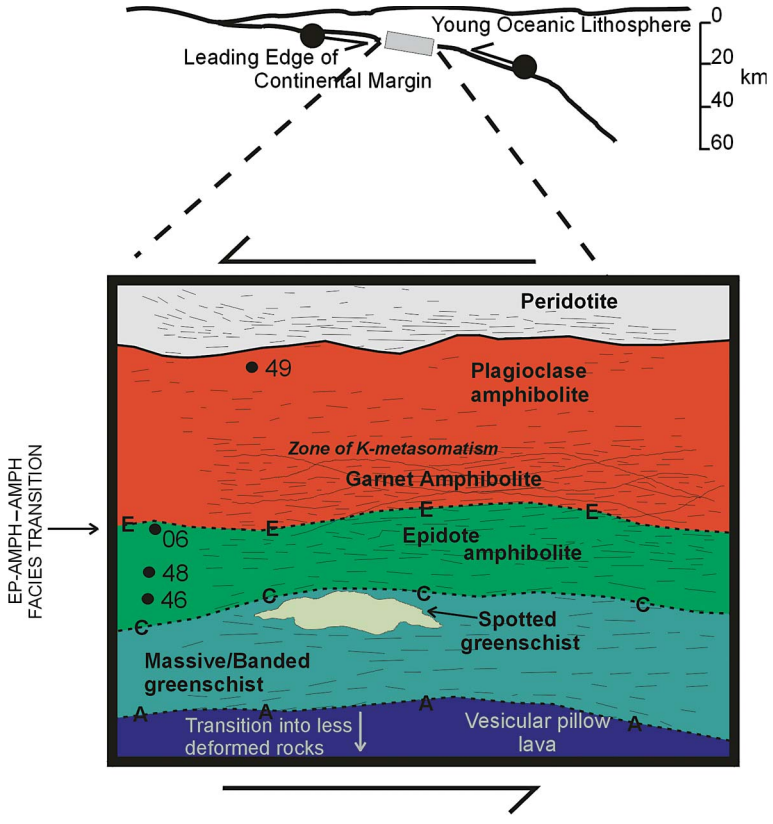


FIG. 1. Schematic cross-section showing the assembly of the St. Anthony Complex within a high-temperature ductile shear-zone and the metamorphic field-gradient in the metamorphic sole (after Jamieson 1986). The tectonic setting is inferred to have been in the upper part of a subduction zone, illustrated schematically at the top of the diagram. Dashed lines labeled A, C and E represent actinolite-in, chlorite-out and epidote-out isograds, respectively. Schematic locations of samples 46, 48, 06 and 49 are shown.

Plagioclase is partially saussuritized, and matrix quartz occurs as granular aggregates. Epidote is present in the matrix of some samples, but in others, it is concentrated in fine-grained aggregates with minor carbonate and amphibole forming a separate compositional domain. The *plagioclase amphibolite* (Fig. 2b) is a medium- to coarse-grained rock consisting of Ca amphibole, also with olive green to brown pleochroism and inclusions of quartz and titanite, interlayered with plagioclase, quartz and minor titanite. Plagioclase occurs as large anhedral, saussuritized grains and as fine-grained crystals in the matrix, some of which exhibit deformation twins, and fine-grained rhombic titanite is a minor modal phase. The main fabric in these rocks is a foliation defined by the alignment of Ca amphibole and plagioclase. We have excluded garnet amphibolite from this study, although the lithology is present within the metamorphic sole of the St Anthony Complex (Fig. 1), because it has different whole-rock major- and trace-element ccomposition, inferred to be due to metasomatism (Jamieson & Strong 1978, Jamieson 1979); as a result, its mineralogy cannot readily be compared with that in the sample suite.

Petrographic evidence for within-grain zoning in the sample suite is limited. On the basis of its homogeneous pleochroic color under the petrographic microscope, the calcic amphibole seems largely unzoned (Fig. 2b), but individual crystals of epidote commonly exhibit variable birefringence (Fig. 2a). Under BSE imaging, however, zoning effects are more readily observed, and lighter grey patches and rims are apparent in some hornblende grains (Fig. 2c), and epidote is observed to be pervasively patchily zoned on the 5–10 μm scale (Fig. 2d).

On the basis of the observed assemblages and qualitative ED analyses, the metamorphic reaction that occurred at the epidote-out isograd is:

$$\text{Ca Amp}_1 + \text{Pl}_1 + \text{Ep} + \text{Ttn}_1 \pm \text{Qtz} \leftrightarrow \text{Ca Amp}_2 + \text{Pl}_2 + \text{Ttn}_2 \pm \text{Qtz} + \text{H}_2\text{O} \quad \text{R1},$$

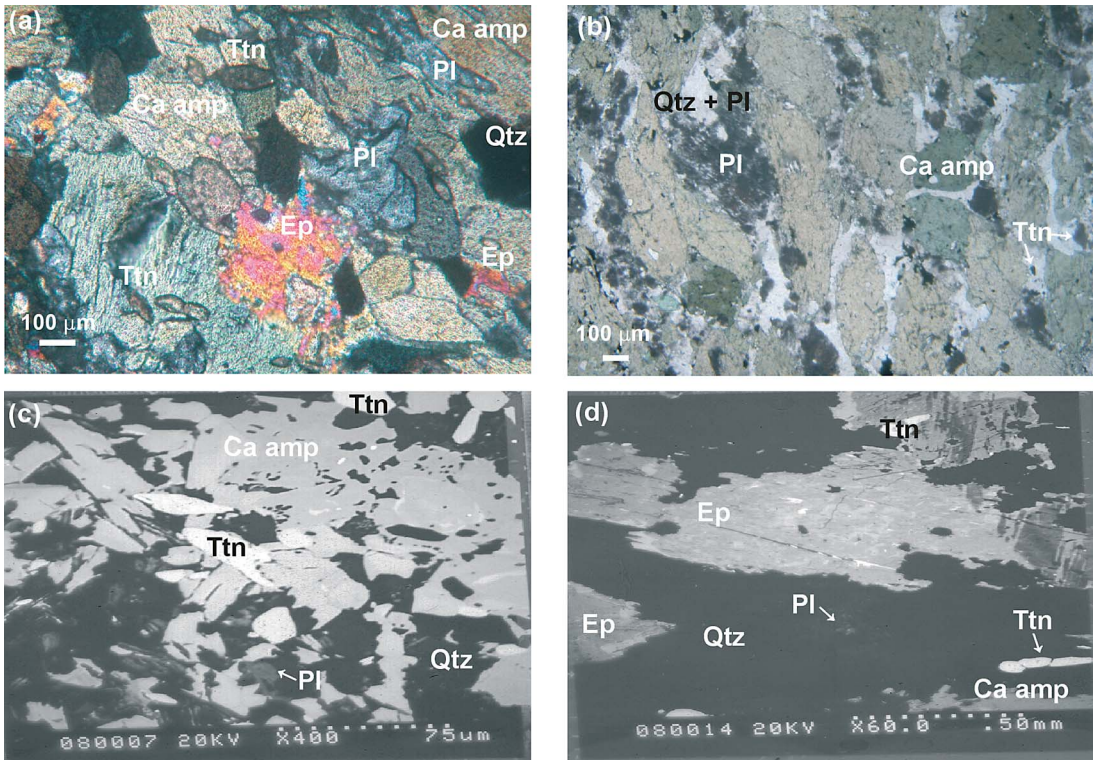


FIG. 2. Representative photomicrographs and BSE images of analyzed metabasic rocks. a) Epidote amphibolite from the Goose Cove Schist below the epidote-out isograd (XPL). b) Plagioclase amphibolite from the Green Ridge Amphibolite above the epidote-out isograd (PPL). c) BSE image showing zoning in Ca amphibole. d) BSE image of epidote showing patchy zoning. Mineral symbols after Kretz (1983).

which implies that components in epidote were largely taken up by slight adjustments in the compositions and modal abundances of Ca amphibole, plagioclase, and possibly the titanite, such that $Pl_2$ is more An-rich than $Pl_1$, and Ca $Amp_2$ is more aluminous than Ca $Amp_1$.

## Results

### *Whole-rock composition*

Results of whole-rock major- and trace-element analyses of eight metabasic rocks are presented in Table 1. MgO varies from approximately 6 to 12 wt% and shows correlations with several other oxides (*e.g.*, $SiO_2$, FeO, $Fe_2O_3$, $Na_2O$; Mulrooney 2004). Samples analyzed in this study, together with compositions reported by Jamieson (1979), cluster in ACF composition space (Fig. 3a), suggesting that they form part of a coherent geochemical suite that experienced limited differentiation. A similar conclusion may be drawn from the overlapping chondrite-normalized whole-rock REE patterns (Fig. 3b). In detail, Figure 3a shows that the sample suite, including the four samples that are the main focus of this paper, can be subdivided into two compositional subgroups based on small differences in CaO content, denoted as A (samples 46 and 48) and B (samples 06 and 49). Subgroup A, which comprises two samples of epidote amphibolite, is slightly more calcic than subgroup B, which includes epidote amphibolite (06) and plagioclase amphibolite (49), suggesting that the presence and the modal abundance of epidote may have been controlled by bulk CaO to some extent. The very similar chondrite-normalized bulk-rock REE contents of the four samples (Fig. 3b) imply that metamorphism was essentially isochemical with respect to the REE.

TABLE 1. WHOLE-ROCK COMPOSITIONS OF METAMAFIC ROCKS FROM THE ST. ANTHONY COMPLEX, NEWFOUNDLAND, WITH DATA ON THE RARE-EARTH ELEMENTS

| Sample | 06 | 46 | 47 | 48 | 49 | 50 | 69 | 70 |
|---|---|---|---|---|---|---|---|---|
| Grade | EA | EA | PA | EA | PA | PA | GS | GS |
| $SiO_2$ wt% | 47.79 | 44.45 | 45.05 | 45.85 | 44.16 | 45.71 | 48.42 | 47.93 |
| $Al_2O_3$ | 11.63 | 12.32 | 11.74 | 13.01 | 10.84 | 11.71 | 11.41 | 10.31 |
| $TiO_2$ | 1.74 | 1.92 | 1.70 | 1.77 | 1.66 | 1.63 | 2.06 | 1.88 |
| FeO | 8.73 | 8.95 | 10.18 | 6.72 | 10.24 | 12.81 | 7.51 | 8.28 |
| $Fe_2O_3$ | 4.61 | 5.32 | 4.22 | 6.11 | 3.61 | | 7.02 | 5.36 |
| MgO | 9.22 | 7.47 | 11.51 | 6.99 | 9.84 | 11.10 | 6.64 | 6.94 |
| MnO | 0.23 | 0.28 | 0.22 | 0.26 | 0.22 | 0.20 | 0.23 | 0.21 |
| CaO | 9.67 | 12.49 | 7.06 | 13.34 | 8.57 | 10.18 | 11.13 | 12.39 |
| $Na_2O$ | 2.33 | 2.39 | 2.10 | 2.65 | 2.74 | 2.20 | 3.07 | 2.71 |
| $K_2O$ | 0.21 | 0.87 | 0.29 | 0.66 | 0.28 | 0.23 | 0.55 | 0.56 |
| $P_2O_5$ | 0.18 | 0.20 | 0.16 | 0.18 | 0.12 | 0.20 | 0.18 | 0.14 |
| Total | 96.34 | 96.66 | 94.23 | 97.54 | 92.28 | 95.97 | 98.22 | 96.71 |
| La ppm | 5 | 5 | 5 | 6 | 5 | 5 | 4 | 4 |
| Ce | 14 | 16 | 14 | 16 | 14 | 15 | 13 | 12 |
| Pr | 2 | 2 | 2 | 2 | 2 | 2 | 2 | 2 |
| Nd | 12 | 12 | 12 | 12 | 12 | 12 | 13 | 12 |
| Sm | 4 | 4 | 4 | 4 | 4 | 4 | 5 | 4 |
| Eu | 1 | 2 | 1 | 1 | 1 | 1 | 2 | 2 |
| Gd | 6 | 6 | 6 | 5 | 5 | 6 | 7 | 6 |
| Tb | 1 | 1 | 1 | 1 | 1 | 1 | 1 | 1 |
| Dy | 7 | 7 | 7 | 6 | 6 | 6 | 8 | 7 |
| Ho | 1 | 1 | 1 | 1 | 1 | 1 | 2 | 1 |
| Er | 4 | 4 | 4 | 4 | 4 | 4 | 5 | 4 |
| Tm | 1 | 1 | 1 | 1 | 1 | 1 | 1 | 1 |
| Yb | 4 | 4 | 4 | 3 | 4 | 4 | 5 | 4 |
| Lu | 1 | 1 | 1 | 1 | 1 | 1 | 1 | 1 |
| La/Lu | 5 | 5 | 5 | 6 | 5 | 5 | 4 | 4 |
| Eu/Eu* | 0.63 | 1.26 | 0.63 | 0.69 | 0.69 | 0.63 | 1.04 | 1.26 |

The proportion of major elements was established by X-ray-fluorescence analysis. Levels of concentration of the rare-earth elements were determined by solution ICP–MS. Rock names: GS: greenschist, EA: epidote amphibolite, PA: plagioclase amphibolite.

### *Composition of the minerals in terms of major elements*

Samples 46, 48 (subgroup A), and 06 (subgroup B) are epidote amphibolite and contain 10%, 7% and 3% modal epidote, respectively, whereas sample 49 (subgroup B) is a plagioclase amphibolite from above the isograd and is epidote-free (Fig. 1). Although BSE images indicate the presence of zoning in Ca amphibole and epidote, the scale is too small for analysis by LAM–ICP–MS, such that major-element concentrations and structural formulae for the four samples are presented as averages in Table 2. Cation site-occupancies are based on the number and size of specific sites in the phase of interest (Smith & Brown 1987, Smyth & Bish 1988) and the ionic radius and charge of the substituting cation (Shannon 1976).

*Ca amphibole* is the most abundant phase investigated, generally occurring as medium to coarse grains. Compositions in terms of oxide weight % were normalized to 23 atoms of oxygen per formula unit (*apfu*), yielding cation totals in the range of 15.50 to 15.80 *apfu*. In terms of the Ca–Mg–Fe diagram (Fig. 4a), the compositions confirm the petrographic interpretation that all analyzed amphibole is calcic, but indicate that there are two groups in different samples with significantly different amounts of cummingtonite in solid solution, *i.e.*, a cummingtonite-poor group with $X_{Cum}^{Amp} \approx 0.03$, and a cummingtonite-rich group in which $X_{Cum}^{Amp} \approx 0.12$, near the limit of substitution of (Mg,Fe) for Ca, according to Spear (1993). The nomenclature of "hornblende-like" amphiboles such as these is based on the number of Na + K atoms at *A* sites *versus* the number of Si atoms at tetrahedral sites (Fig. 4b; Leake 1997, Leake *et al.* 2003). Analyzed grains contain >0.5 $^{A}$(Na + K) *apfu* and between 1.5 and 2 $^{IV}$Al *apfu*, forming two clusters situated slightly below a line joining tremolite and pargasite. The restricted scatter of the analytical data confirms the interpretation from the BSE images that within-sample zoning of the Ca amphibole is limited.

*Plagioclase* is stable across the entire suite of samples as a fine- to medium-grained phase with ubiquitous partial sericitization. Compositions were normalized to eight *apfu* oxygen, yielding cation totals near 5.00 *apfu*. The compositions show that *Or* is a very

TABLE 2. AVERAGE MAJOR-ELEMENT COMPOSITIONS AND STRUCTURAL FORMULAE OF Ca AMPHIBOLE, PLAGIOCLASE, EPIDOTE AND TITANITE IN METAMAFIC ROCKS FROM THE ST. ANTHONY COMPLEX, NEWFOUNDLAND

| Ca amp | 46 | | 48 | | 49 | | 06 | |
|---|---|---|---|---|---|---|---|---|
| *n* | 4 | | 4 | | 4 | | 4 | |
| $SiO_2$ wt% | 43.37 | 0.43 | 44.48 | 0.52 | 41.40 | 0.16 | 41.77 | 0.65 |
| $TiO_2$ | 1.01 | 0.07 | 0.86 | 0.14 | 1.10 | 0.04 | 1.05 | 0.10 |
| $Al_2O_3$ | 11.88 | 0.40 | 12.89 | 0.39 | 12.78 | 0.20 | 12.33 | 0.25 |
| FeO | 15.62 | 0.27 | 15.57 | 0.26 | 19.63 | 0.28 | 19.75 | 0.39 |
| MnO | 0.29 | 0.03 | 0.44 | 0.06 | 0.41 | 0.07 | 0.41 | 0.06 |
| MgO | 11.17 | 0.24 | 11.07 | 0.16 | 8.75 | 0.15 | 8.86 | 0.22 |
| CaO | 10.89 | 0.09 | 11.25 | 0.09 | 12.07 | 0.10 | 11.93 | 0.16 |
| $Na_2O$ | 1.99 | 0.12 | 1.95 | 0.09 | 1.79 | 0.07 | 1.86 | 0.02 |
| $K_2O$ | 0.12 | 0.06 | 0.15 | 0.03 | 1.40 | 0.05 | 1.28 | 0.06 |
| Total | 96.32 | | 98.66 | | 99.32 | | 99.24 | |
| *T* site | | | | | | | | |
| Si *apfu* | 6.52 | | 6.52 | | 6.21 | | 6.27 | |
| $^{IV}$Al | 1.48 | | 1.48 | | 1.79 | | 1.58 | |
| Total | 8.00 | | 8.00 | | 8.00 | | 8.00 | |
| *M*1–3 sites | | | | | | | | |
| $^{VI}$Al | 0.63 | | 0.74 | | 0.47 | | 0.45 | |
| $Fe^{3+}$ | 0.02 | | | | 0.29 | | 0.26 | |
| Ti | 0.11 | | 0.10 | | 0.12 | | 0.12 | |
| Fe, Mg | 4.24 | | 4.16 | | 4.12 | | 4.17 | |
| Total | 5.00 | | 5.00 | | 5.00 | | 5.00 | |
| *M*4 site | | | | | | | | |
| Fe, Mg | 0.24 | | 0.22 | | 0.06 | | 0.08 | |
| Ca | 1.76 | | 1.77 | | 1.94 | | 1.92 | |
| Na | | | 0.01 | | | | | |
| Total | 2.00 | | 2.00 | | 2.00 | | 2.00 | |
| *A* site | | | | | | | | |
| Na | 0.58 | | 0.54 | | 0.52 | | 0.54 | |
| K | 0.03 | | 0.03 | | 0.27 | | 0.25 | |
| Total | 0.61 | | 0.56 | | 0.79 | | 0.79 | |
| Σcations | 15.61 | | 15.56 | | 15.79 | | 15.79 | |
| *X* Mg | 0.56 | | 0.56 | | 0.47 | | 0.47 | |
| *X* Fe | 0.44 | | 0.44 | | 0.53 | | 0.53 | |
| *X*(Cum) | 0.12 | | 0.11 | | 0.03 | | 0.04 | |

| Plagioclase | 46 | | 48 | | 49 | | 06 | |
|---|---|---|---|---|---|---|---|---|
| *n* | 4 | | 4 | | 4 | | 4 | |
| $SiO_2$ wt% | 59.93 | 1.54 | 59.59 | 1.12 | 56.00 | 1.16 | 57.90 | 0.30 |
| $TiO_2$ | <D.L. | 0.08 | 0.05 | <D.L. | 0.07 | 0.04 | | |
| $Al_2O_3$ | 25.10 | 1.30 | 26.28 | 0.22 | 25.93 | 0.97 | 26.49 | 0.24 |
| FeO | 0.58 | 0.55 | 0.27 | 0.07 | 0.62 | 0.27 | 0.19 | 0.10 |
| MnO | <D.L. | | <D.L. | | <D.L. | | <D.L. | |
| MgO | 0.06 | 0.04 | <D.L. | | 0.09 | 0.08 | 0.04 | 0.02 |
| CaO | 7.10 | 0.64 | 7.49 | 0.44 | 9.87 | 0.32 | 8.71 | 0.44 |
| $Na_2O$ | 7.84 | 0.60 | 7.17 | 0.21 | 5.29 | 0.39 | 6.60 | 0.12 |
| $K_2O$ | 0.22 | 0.20 | 0.31 | 0.22 | 0.07 | 0.04 | 0.06 | 0.02 |
| Total | 100.8 | | 101.2 | | 97.9 | | 100.1 | |
| *T* site | | | | | | | | |
| Si *apfu* | 2.66 | | 2.63 | | 2.57 | | 2.59 | |
| Al | 1.31 | | 1.37 | | 1.40 | | 1.40 | |
| Fe | 0.02 | | 0.01 | | 0.02 | | 0.003 | |
| Mg | 0.002 | | | | 0.01 | | | |
| Total | 4.00 | | 4.01 | | 4.00 | | 4.00 | |
| *A* site | | | | | | | | |
| Ca | 0.34 | | 0.35 | | 0.48 | | 0.42 | |
| Na | 0.68 | | 0.61 | | 0.47 | | 0.57 | |
| K | 0.01 | | 0.02 | | 0.002 | | 0.001 | |
| Total | 1.02 | | 0.98 | | 0.96 | | 0.99 | |
| ΣCations | 5.02 | | 4.99 | | 4.96 | | 4.99 | |
| *X* Ca (An) | 0.33 | | 0.37 | | 0.51 | | 0.42 | |
| *X* Na (Ab) | 0.66 | | 0.62 | | 0.49 | | 0.58 | |
| *X* K (Or) | 0.01 | | 0.01 | | | | | |

| Epidote | 06 | | 46 | | 48 | |
|---|---|---|---|---|---|---|
| *n* | 4 | | 4 | | 3 | |
| $SiO_2$ wt% | 40.08 | 0.34 | 38.02 | 0.45 | 40.27 | 0.23 |
| $TiO_2$ | <D.L. | | 0.16 | 0.08 | 0.10 | 0.02 |
| $Al_2O_3$ | 29.80 | 0.93 | 24.09 | 0.28 | 25.64 | 0.38 |
| $Fe_2O_3$ | 5.68 | 1.07 | 11.93 | 0.47 | 10.40 | 0.63 |
| $Mn_2O_3$ | 0.12 | 0.09 | 0.09 | 0.04 | 0.16 | 0.04 |
| MgO | 0.09 | 0.06 | 0.17 | 0.04 | <D.L. | |
| CaO | 24.53 | 0.06 | 23.44 | 0.27 | 23.47 | 0.25 |
| $Na_2O$ | 0.09 | 0.09 | 0.10 | 0.07 | 0.32 | 0.10 |
| $K_2O$ | <D.L. | | <D.L. | | <D.L. | |
| Total | 100.29 | | 97.84 | | 100.04 | |
| *T* site | | | | | | |
| Si *apfu* | 3.05 | | 3.08 | | 3.14 | |
| Total | 3.05 | | 3.08 | | 3.14 | |
| *M*1–3 sites | | | | | | |
| Ti | | | 0.02 | | | |
| Al | 2.67 | | 2.30 | | 2.36 | |
| $Fe^{3+}$ | 0.36 | | 0.81 | | 0.68 | |
| Mn | 0.01 | | 0.01 | | 0.01 | |
| Mg | 0.01 | | | | | |
| Total | 3.05 | | 3.12 | | 3.07 | |
| *X* site | | | | | | |
| Ca | 2.00 | | 2.03 | | 1.96 | |
| Na | 0.01 | | 0.01 | | 0.05 | |
| K | | | | | | |
| Total | 2.01 | | 2.04 | | 2.01 | |
| ΣCations | 8.11 | | 8.24 | | 8.22 | |
| *X* Al (Czo) | 0.64 | | 0.25 | | 0.34 | |
| *X* Fe (Ep) | 0.35 | | 0.72 | | 0.64 | |
| *X* Mn (Pm) | 0.01 | | 0.03 | | 0.02 | |

| Titanite | 46 | | 48 | | 49 | | 06 | |
|---|---|---|---|---|---|---|---|---|
| *n* | 3 | | 3 | | 2 | | 3 | |
| $SiO_2$ wt% | 30.13 | 0.05 | 31.02 | 0.07 | 30.31 | 0.11 | 30.44 | 0.28 |
| $TiO_2$ | 37.79 | 0.06 | 38.46 | 0.38 | 37.40 | 0.47 | 36.09 | 0.45 |
| $Al_2O_3$ | 1.37 | 0.08 | 1.25 | 0.19 | 1.89 | 0.11 | 1.67 | 0.25 |
| $Fe_2O_3$ | 0.99 | 0.05 | 0.95 | 0.06 | 0.75 | 0.17 | 1.58 | 0.28 |
| $Mn_2O_3$ | 0.13 | 0.05 | <D.L. | | 0.07 | 0.03 | 0.15 | 0.03 |
| MgO | 0.05 | 0.03 | 0.05 | 0.06 | <D.L. | | 0.05 | 0.01 |
| CaO | 28.54 | 0.15 | 29.00 | 0.08 | 28.16 | 0.26 | 28.08 | 0.29 |
| $Na_2O$ | 0.06 | 0.04 | 0.01 | 0.01 | <D.L | | 0.14 | 0.11 |
| $K_2O$ | 0.01. | | 0.01 | 0.01 | <D.L | | 0.01 | 0.01 |
| Total | 98.83 | | 100.67 | | 98.52 | | 97.98 | |
| *T* site | | | | | | | | |
| Si *apfu* | 3.99 | | 4.03 | | 4.01 | | 4.06 | |
| Total | 3.99 | | 4.03 | | 4.01 | | 4.06 | |
| *M* site | | | | | | | | |
| Ti | 3.76 | | 3.75 | | 3.72 | | 3.62 | |
| Al | 0.21 | | 0.20 | | 0.28 | | 0.26 | |
| $Fe^{3+}$ | 0.03 | | 0.05 | | | | 0.12 | |
| $Mn^{3+}$ | | | | | | | | |
| Total | 4.00 | | 4.00 | | 4.00 | | 4.00 | |
| *A* site | | | | | | | | |
| $Fe^{2+}$ | | | 0.03 | | 0.05 | | 0.01 | |
| Mg | 0.05 | | 0.01 | | | | | |
| Ca | 4.05 | | 4.03 | | 3.99 | | 4.02 | |
| Na | 0.01 | | | | | | 0.03 | |
| K | | | | | | | | |
| Total | 4.10 | | 4.07 | | 4.05 | | 4.04 | |
| ΣCations | 12.09 | | 12.10 | | 12.06 | | 12.10 | |
| *X* Ti | 0.76 | | 0.75 | | 0.72 | | 0.62 | |
| *X* Al | 0.21 | | 0.20 | | 0.28 | | 0.26 | |
| *X* $Fe^{3+}$ | 0.03 | | 0.05 | | | | 0.12 | |

For each sample, the wt% oxide is shown with ± one standard deviation in the following column. *n*: number of analyses.

minor component, and that *An* increases across the epidote-out isograd from approximately $An_{33}$ to $An_{51}$ (Fig. 4c). Within-sample zoning appears to be minor ($An_{\pm 0.05}$).

*Epidote* occurs as a fine- to medium-grained matrix phase and in separate epidote-rich domains. To ensure that equilibrium was achieved with the other phases, only matrix grains were analyzed in this study. Compositions were normalized to 12.5 *apfu* oxygen, giving cation totals near 8.00 *apfu*. The clinozoisite – epidote – piemontite plot, shown in Figure 4d (after Ercit 2002), illustrates that *Pm* is negligible in the grains analyzed, which have compositions in the range $Czo_{25-64}$. Within-sample zoning in epidote is the greatest of all the analyzed phases, and is especially apparent in sample 06 (Fig. 4d).

*Titanite* is present primarily as a fine-grained subhedral to euhedral matrix phase. Compositions were normalized to 20 *apfu* oxygen, giving cation totals of approximately 12 *apfu*. Compositions are plotted on the basis of Ti–Al–$Fe^{3+}$ proportions in octahedral sites in Figure 4e, which shows that there is 5–10% Al and <5% $Fe^{3+}$ in the analyzed grains and that within-sample compositional variation is limited.

Figure 4 also shows that the compositions of Ca amphibole, plagioclase, epidote and titanite are all dependent to some degree on the bulk composition, being slightly different in compositional subgroups A and B.

*Mineral compositions in terms of the REE*

Average REE concentrations of the four coexisting phases are presented in Table 3, together with the sums of LREE (La–Nd), MREE (Sm–Nd), and HREE (Er–Lu), La/Lu values and Eu anomalies. Mineral compositions on the basis of L-, M-, and HREE abundance and chondrite-normalized REE diagrams are shown in Figures 5 and 6, respectively.

*Ca amphibole* exhibits low to moderate concentrations of REE (ΣREE in the range 6–66 ppm), with higher values in "cummingtonite-poor" compositions. All grains of Ca amphibole have slightly higher abundances of LREE and MREE relative to HREE, with "cummingtonite-poor" amphibole being relatively more LREE-enriched (Fig. 5a). Chondrite-normalized REE patterns for "cummingtonite-rich" amphibole have approximately chondritic abundances and exhibit moderate LREE depletion, with small negative Eu anomalies, whereas those for "cummingtonite-poor" amphibole have concentrations approximately 10 times chondrite and are flatter, with smaller Eu anomalies (Fig. 6a). There is a corresponding change in the La/Lu values, with those for "cummingtonite-rich" amphibole being near unity and those for "cummingtonite-poor" amphibole ranging from 3 to 5. Thus the type of Ca amphibole, its REE concentration, LREE:HREE ratio, and the size of the Eu anomaly all change between subgroups A and B.

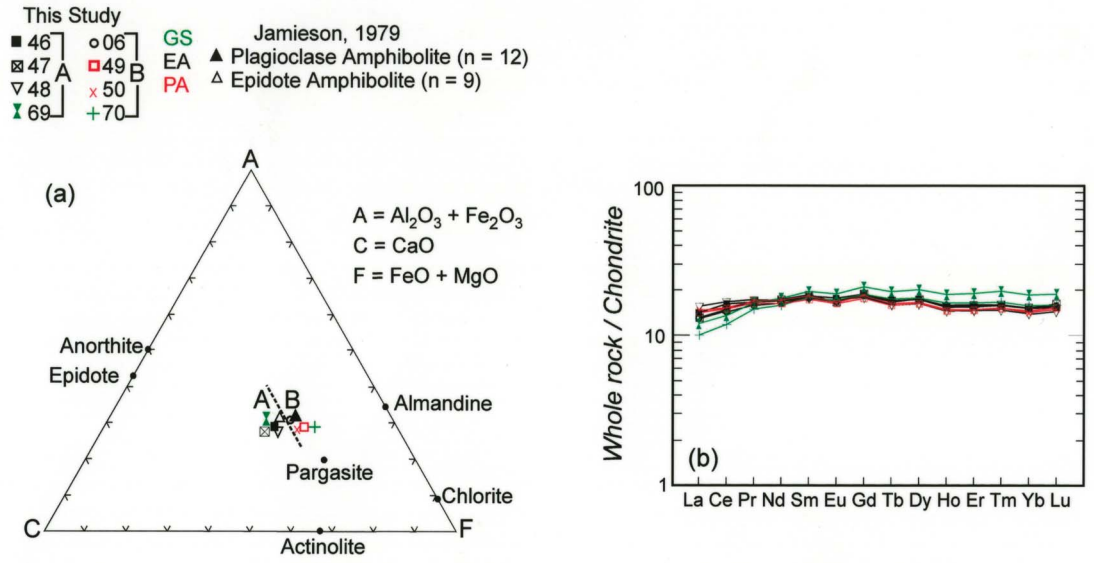


FIG. 3. (a) ACF diagram showing the compositions (from whole-rock analyses) of samples used in this study and those taken from Jamieson (1979). End-member compositions of common minerals in metamafic rocks at greenschist and amphibolite facies also are shown. A and B refer to two compositional subgroups defined in the text. (b) Chondrite-normalized, whole-rock REE patterns of analyzed samples; chondrite values from Taylor & McLennan (1985). Samples 69 and 70 are greenschists (GS), 06, 46 and 48 are epidote amphibolites (EA), and 47, 49 and 50 are plagioclase amphibolites (PA).

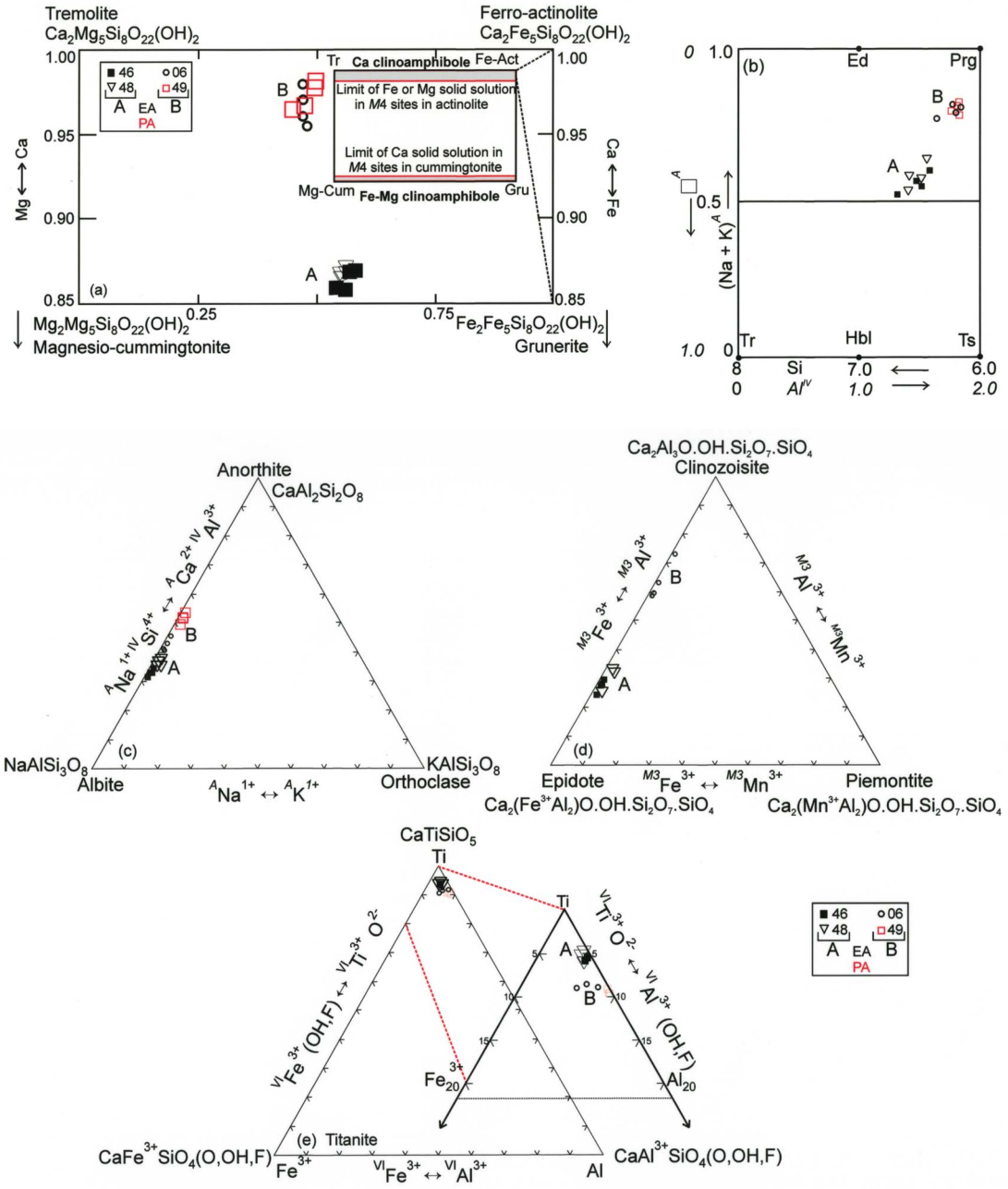


FIG. 4. Compositional phase-diagrams illustrating major-element variations of Ca amphibole, plagioclase, epidote and titanite from four samples across the epidote-out isograd. EA: epidote amphibolite, PA: plagioclase amphibolite; A and B refer to bulk-composition subgroups defined in the text and Fig. 3a. a) Ca–Fe–Mg clinoamphibole composition space showing analyzed samples, exchange vectors and limits of solid solutions in Ca and Mg,Fe amphiboles (after Spear 1993). b) Nomenclature of Ca amphiboles expressed as numbers of $^{A}$(Na + K) and $^{IV}$Al *apfu* (after Leake *et al.* 1997, 2003). $^{A}\square$ represents a vacancy at the *A* site. Mineral symbols after Kretz (1983). c) Plagioclase compositions plotted in Ab–An–Or composition space. d) Epidote compositions plotted in Czo–Ep–Pm composition space on the basis of the numbers of octahedrally coordinated Al, Fe and Mn cation totals at one of the three *Y* sites. e) Titanite compositions on the basis of octahedrally coordinated $Fe^{3+}$, Ti and Al.

*Plagioclase* has the lowest ΣREE of all analyzed phases (ΣREE in the range 1–14 ppm), with no consistent trend of ΣREE abundance across the epidote-out isograd (Table 3), but normalized LREE proportions are greater in subgroup B (Fig. 5b). Chondrite-normalized REE patterns are LREE-enriched, with large positive Eu anomalies (Fig. 6b). Measured HREE abundances are irregular because the concentrations for some elements approach detection limits, and the LREE:HREE ratio, expressed as Ce/Yb because of Lu concentrations below detection limits in some samples, ranges from approximately 6 up to 60 (Table 3). There is a positive correlation between the (LREE + MREE):HREE ratio and $X_{An}^{Pl}$ (*cf.* Figs. 4c, 5b).

The analyzed *epidote* contains moderate concentrations of REE, ranging from approximately 80 to 375 ppm, with the highest concentration in sample 06 from just below the epidote-out isograd. The La:Lu ratios,

TABLE 3. AVERAGE REE CONCENTRATIONS, ΣREE, La:Lu RATIOS, AND Eu ANOMALIES IN Ca AMPHIBOLE, PLAGIOCLASE, EPIDOTE AND TITANITE IN METAMAFIC ROCKS FROM THE ST. ANTHONY COMPLEX, NEWFOUNDLAND

| Plagioclase | 46 | | 48 | | 49 | | 06 | |
|---|---|---|---|---|---|---|---|---|
| *n* | 4 | | 4 | | 4 | | 4 | |
| La ppm | 0.28 | 0.20 | 0.59 | 0.16 | 1.82 | 0.93 | 3.74 | 1.26 |
| Ce | 0.38 | 0.21 | 0.90 | 0.41 | 1.85 | 0.99 | 7.08 | 1.97 |
| Pr | 0.04 | 0.01 | 0.21 | 0.09 | 0.16 | 0.08 | 0.50 | 0.10 |
| Nd | 0.12 | 0.04 | 0.82 | 0.49 | 0.50 | 0.34 | 1.31 | 0.32 |
| Sm | 0.04 | 0.01 | 0.23 | 0.04 | 0.07 | 0.05 | 0.23 | 0.04 |
| Eu | 0.09 | 0.03 | 1.64 | 0.43 | 0.11 | 0.05 | 0.22 | 0.04 |
| Gd | 0.04 | 0.01 | 0.24 | 0.08 | 0.03 | 0.02 | 0.15 | 0.03 |
| Tb | | | 0.04 | 0.01 | 0.01 | 0.01 | 0.02 | 0.01 |
| Dy | 0.02 | 0.01 | 0.17 | 0.04 | 0.03 | 0.02 | 0.22 | 0.07 |
| Ho | | | 0.04 | 0.01 | 0.01 | 0.01 | 0.03 | 0.01 |
| Er | 0.02 | 0.01 | 0.10 | 0.06 | 0.03 | 0.01 | 0.06 | 0.02 |
| Tm | | | 0.02 | 0.01 | 0.01 | 0.01 | 0.02 | 0.01 |
| Yb | 0.03 | 0.01 | 0.10 | 0.02 | 0.03 | 0.02 | 0.13 | 0.07 |
| Lu | | | 0.03 | 0.01 | | | 0.01 | 0.01 |
| Σ REE | 1.07 | | 5.14 | | 4.65 | | 13.73 | |
| LREE (La–Nd) | 0.82 | | 2.52 | | 4.33 | | 12.63 | |
| MREE (Sm–Ho) | 0.19 | | 2.37 | | 0.25 | | 0.87 | |
| HREE (Er–Lu) | 0.06 | | 0.25 | | 0.07 | | 0.23 | |
| *Ce/Yb | 12.67 | | 5.9 | | 60.67 | | 54.46 | |
| Eu/Eu* | 6.86 | | 21.18 | | 7.53 | | 3.55 | |

| Epidote | 06 | | 46 | | 48 | |
|---|---|---|---|---|---|---|
| *n* | 4 | | 4 | | 3 | |
| La ppm | 76.33 | 27.03 | 35.83 | 21.14 | 10.67 | 8.64 |
| Ce | 166.8 | 59.40 | 69.38 | 37.26 | 31.69 | 29.41 |
| Pr | 19.05 | 6.93 | 9.00 | 5.10 | 4.15 | 3.90 |
| Nd | 72.65 | 28.85 | 36.40 | 20.07 | 17.75 | 15.84 |
| Sm | 13.91 | 4.39 | 6.78 | 3.51 | 4.20 | 3.62 |
| Eu | 4.87 | 0.98 | 2.38 | 1.48 | 1.43 | 1.23 |
| Gd | 10.41 | 2.73 | 5.06 | 2.46 | 3.09 | 2.41 |
| Tb | 1.43 | 0.23 | 0.68 | 0.25 | 0.45 | 0.25 |
| Dy | 8.12 | 1.32 | 4.15 | 1.25 | 2.60 | 1.88 |
| Ho | 1.40 | 0.16 | 0.75 | 0.14 | 0.49 | 0.35 |
| Er | 3.33 | 0.55 | 2.02 | 0.35 | 1.32 | 0.93 |
| Tm | 0.42 | 0.09 | 0.26 | 0.05 | 0.17 | 0.12 |
| Yb | 2.72 | 0.64 | 1.75 | 0.31 | 1.25 | 0.94 |
| Lu | 0.36 | 0.09 | 0.26 | 0.05 | 0.18 | 0.12 |
| Σ REE | 381.8 | | 174.7 | | 79.42 | |
| LREE (La–Nd) | 334.8 | | 150.6 | | 64.25 | |
| MREE (Sm–Ho) | 40.14 | | 19.81 | | 12.25 | |
| HREE (Er–Lu) | 6.83 | | 4.28 | | 2.92 | |
| La/Lu | 212.0 | | 137.8 | | 59.27 | |
| Eu/Eu* | 1.24 | | 1.24 | | 1.21 | |

| Ca amphibole | 46 | | 48 | | 49 | | 06 | |
|---|---|---|---|---|---|---|---|---|
| *n* | 4 | | 4 | | 4 | | 4 | |
| La ppm | 0.22 | 0.02 | 0.10 | 0.02 | 3.81 | 0.17 | 2.79 | 0.98 |
| Ce | 1.18 | 0.18 | 0.57 | 0.07 | 13.00 | 0.84 | 11.76 | 3.07 |
| Pr | 0.22 | 0.03 | 0.14 | 0.02 | 2.27 | 0.11 | 2.25 | 0.40 |
| Nd | 1.44 | 0.02 | 0.96 | 0.16 | 13.08 | 0.30 | 13.70 | 2.17 |
| Sm | 0.66 | 0.02 | 0.56 | 0.10 | 4.63 | 0.11 | 5.07 | 0.58 |
| Eu | 0.23 | 0.03 | 0.15 | 0.02 | 1.54 | 0.08 | 1.79 | 0.25 |
| Gd | 1.12 | 0.10 | 0.98 | 0.14 | 6.55 | 0.20 | 6.76 | 0.57 |
| Tb | 0.19 | 0.02 | 0.18 | 0.02 | 1.10 | 0.05 | 1.21 | 0.12 |
| Dy | 1.66 | 0.20 | 1.31 | 0.22 | 7.75 | 0.42 | 8.21 | 1.04 |
| Ho | 0.37 | 0.06 | 0.31 | 0.03 | 1.65 | 0.14 | 1.69 | 0.16 |
| Er | 1.15 | 0.17 | 0.90 | 0.10 | 4.82 | 0.42 | 5.06 | 0.49 |
| Tm | 0.17 | 0.04 | 0.14 | 0.02 | 0.71 | 0.07 | 0.74 | 0.11 |
| Yb | 1.24 | 0.24 | 0.95 | 0.10 | 4.96 | 0.46 | 5.26 | 0.98 |
| Lu | 0.21 | 0.06 | 0.17 | 0.02 | 0.78 | 0.08 | 0.78 | 0.08 |
| Σ REE | 10.06 | | 7.42 | | 66.63 | | 67.07 | |
| LREE (La–Nd) | 3.06 | | 1.78 | | 32.15 | | 30.50 | |
| MREE (Sm–Ho) | 4.23 | | 3.48 | | 23.21 | | 24.73 | |
| HREE (Er–Lu) | 2.77 | | 2.16 | | 11.27 | | 11.84 | |
| La/Lu | 1.04 | | 0.60 | | 4.88 | | 3.57 | |
| Eu/Eu* | 0.83 | | 0.53 | | 0.83 | | 0.93 | |

| Titanite | 46 | | 48 | | 49 | | 06 | |
|---|---|---|---|---|---|---|---|---|
| *n* | 3 | | 3 | | 2 | | 3 | |
| La ppm | 133.5 | 55.35 | 176.7 | 47.30 | 68.95 | 44.13 | 206.67 | 70.56 |
| Ce | 423.3 | 129.40 | 588.3 | 76.26 | 268.2 | 154.15 | 784.67 | 194.83 |
| Pr | 63.9 | 21.29 | 100.4 | 6.96 | 48.15 | 23.96 | 136.93 | 45.78 |
| Nd | 342.0 | 100.61 | 547.7 | 18.79 | 299.0 | 142.89 | 759.67 | 341.97 |
| Sm | 112.9 | 27.94 | 172.3 | 3.89 | 115.6 | 52.62 | 250.87 | 183.30 |
| Eu | 39.7 | 10.38 | 61.5 | 0.71 | 34.75 | 17.60 | 73.80 | 39.61 |
| Gd | 152.0 | 27.56 | 213.0 | 8.15 | 160.3 | 76.55 | 247.10 | 222.35 |
| Tb | 26.1 | 4.38 | 34.03 | 1.40 | 26.25 | 12.53 | 34.30 | 30.07 |
| Dy | 183.3 | 25.20 | 242.0 | 9.27 | 196.0 | 97.98 | 182.17 | 170.55 |
| Ho | 37.4 | 4.49 | 47.07 | 1.19 | 38.95 | 19.39 | 23.44 | 19.62 |
| Er | 110.6 | 12.93 | 136.0 | 1.14 | 113.5 | 55.11 | 45.39 | 30.69 |
| Tm | 15.53 | 1.99 | 19.03 | 0.57 | 16.51 | 9.23 | 4.57 | 3.43 |
| Yb | 106.3 | 13.38 | 129.3 | 9.23 | 111.1 | 48.91 | 21.73 | 12.72 |
| Lu | 14.50 | 2.20 | 16.70 | 1.85 | 14.78 | 6.30 | 1.94 | 1.28 |
| Σ REE | 1761 | | 2484 | | 1512 | | 2773 | |
| LREE | 962.7 | | 1413 | | 684.3 | | 1887 | |
| MREE | 551.5 | | 769.9 | | 571.8 | | 811.7 | |
| HREE | 246.9 | | 301.0 | | 255.9 | | 73.63 | |
| La/Lu | 8.42 | | 10.57 | | 4.67 | | 106.5 | |
| Eu/Eu* | 0.93 | | 0.99 | | 0.78 | | 0.91 | |

For each sample, the concentration of the rare-earth element is shown with ± one standard deviation in the following column. Blank indicates below detection limit. *n*: number of analyses.

which range from approximately 65 to 330, are highest in Al-rich (clinozoisite-rich) grains in sample 06 (Fig. 5c). Chondrite-normalized patterns for epidote (Fig. 6c) exhibit LREE enrichment, small positive or negative Eu anomalies, and variable REE abundances, from <10 to 150 times chondrite. The within-sample range of REE abundance and type of Eu anomaly suggest that measured compositions differ significantly among grains from the same sample, which is compatible with the patchy zoning pattern illustrated in Figure 2d.

*Titanite*, present primarily as a fine-grained subhedral to euhedral phase in the matrix, is extremely REE-enriched (ΣREE in the range 1500–2400 ppm) and its LREE, MREE and HREE distributions are shown in Figure 5d. Overall, titanite exhibits MREE and LREE enrichment, but titanite in sample 06 is anomalous, displaying variable within-sample LREE enrichment. Most chondrite-normalized REE patterns for titanite (Fig. 6d) exhibit slight depletion in the LREE and relatively flat patterns for MREE and HREE, small negative Eu anomalies, and enrichment of 100 to 1000 times chondrite. Sample 06, an exception, exhibits marked HREE depletion. The La:Lu ratios are between 5 and 10, again with the exception of sample 06, which has a ratio of about 100. The different behavior of sample 06 *may* be attributed to equilibration in the presence of a trace phase such as zircon or xenotime, both of which are known carriers of *HREE* (*e.g.*, Pyle & Spear 1999, Yang & Rivers 2002), although neither phase was observed.

The large positive Eu anomalies in chondrite-normalized plagioclase, the small negative Eu anomalies in chondrite-normalized Ca amphibole and titanite, and the small positive to negative Eu anomalies in chondrite-normalized epidote imply the presence of both $Eu^{2+}$ and $Eu^{3+}$. Preferential substitution of $Eu^{2+}$ into the Ca site in plagioclase, giving rise to a positive Eu anomaly, is well known, and the concomitant negative anomalies in coexisting Ca amphibole and titanite attest to equilibrium

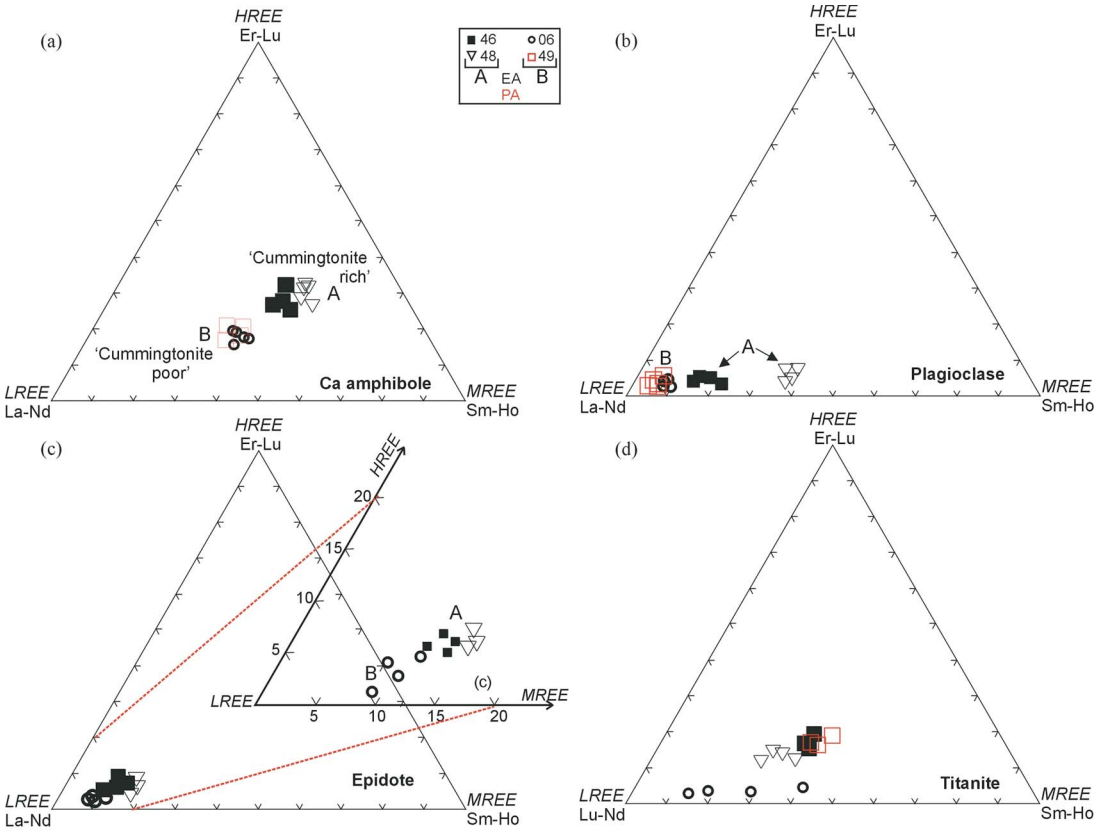


FIG. 5. Average normalized sums of LREE (La–Nd), MREE (Sm–Ho), and HREE (Er–Lu) distributions in: (a) Ca amphibole, (b) plagioclase, (c) epidote, (d) titanite. EA: epidote amphibolite, PA: plagioclase amphibolite; A and B refer to bulk-composition subgroups defined in the text and in Figure 3a.

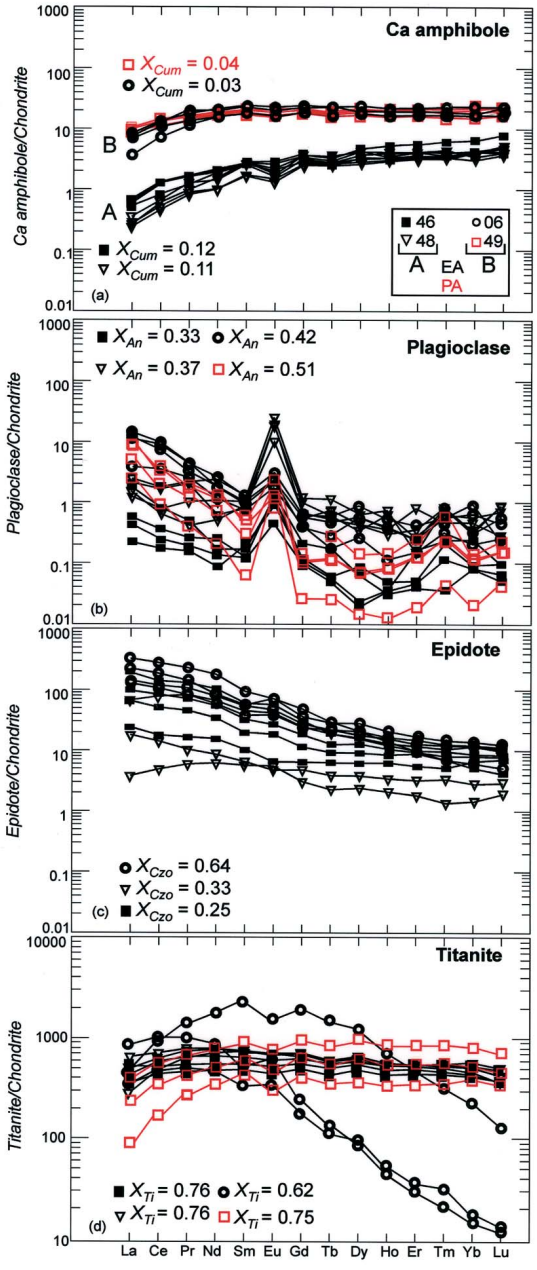


FIG. 6. Chondrite-normalized mineral REE diagrams: (a) Ca amphibole, (b) plagioclase, (c) epidote, (d) titanite. Chondrite-normalization factors from Taylor & McLennan (1985). EA: epidote amphibolite, PA: plagioclase amphibolite, A and B refer to bulk-composition subgroups defined in the text and in Figure 3a.

partitioning during metamorphism. On the assumption that the small negative Eu anomalies in epidote in some samples also indicate equilibrium partitioning, the small positive Eu anomalies in this phase in other samples are probably a reflection of *in situ* replacement of igneous plagioclase by epidote. The smaller negative Eu anomalies in "cummingtonite-poor" compared to "cummingtonite-rich" Ca amphibole suggests that the $Eu^{2+}$ ion is more compatible in the latter phase.

### *Bulk composition and mineral compositions*

In order to explore the possible role of bulk major-element compositional control on epidote stability across the epidote-out isograd, differences in the ratios of the molar proportions of elements that might be expected to exert some control on the modal abundance of epidote were assessed. Figure 7 shows that despite very limited variations in the ratios Ca/(Ca + Na) and $Fe^{3+}$/($Fe^{3+}$ + Al), there is a consistent decline in modal epidote in the vicinity of the epidote-out isograd. This result is compatible with the interpretation that the isograd is indeed a result of changing metamorphic grade, as inferred by Jamieson (1979), even though the isogradic reaction is imposed on samples of slightly variable bulk-composition.

It is also appropriate here to consider the relationship between bulk-rock composition and the major-element composition of the Ca amphibole. Comparison of Figures 3a and 4a shows that the "cummingtonite-rich" Ca amphibole in samples of subgroup A occurs in bulk compositions richer in Ca than "cummingtonite-poor" Ca amphibole in samples of subgroup B, the reverse of

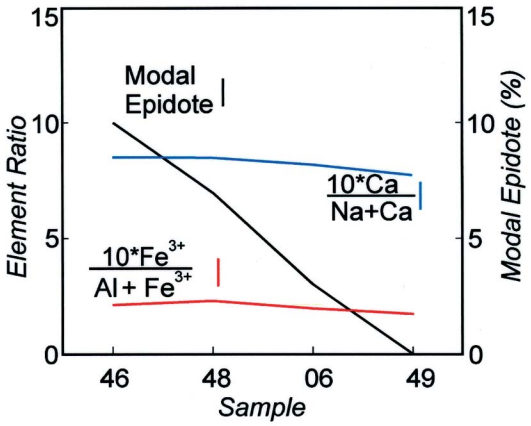


FIG. 7. Plot showing variations in the molar proportions of selected oxide ratios compared to the variation in molar abundance of epidote in four samples across the epidote-out isograd. See text for discussion.

what would be expected. This paradoxical result is interpreted in terms of a changing effective bulk- composition (EBC) available to Ca amphibole during growth, as follows. In relatively calcium-rich bulk-compositions (subgroup A, samples 46 and 48), we infer that early-formed epidote sequestered Ca and Al, thereby depleting the remaining bulk-composition in these elements, leading to passive enrichment of the matrix in Fe and Mg, and the formation of cummingtonite-rich Ca amphibole. In contrast, in relatively calcium-poor bulk-compositions (subgroup B, samples 06 and 49), early crystallization of epidote was suppressed, permitting equilibrium partitioning of Ca among epidote, plagioclase and Ca amphibole, leading to the formation of Ca-rich (cummingtonite-poor) Ca amphibole and Ca enrichment of plagioclase. Thus the effective bulk-composition available to Ca amphibole in bulk composition A was less Ca-rich than the true bulk-composition, lessening the apparent compositional contrast among the samples for this phase. This model implies that epidote nucleated before Ca amphibole in subgroup A, which is consistent with the observation that epidote coexists with chlorite in the absence of Ca amphibole in some greenschist-facies samples. In summary, there are small differences in the bulk compositions of the four samples and of the effective bulk-compositions available to minerals at various stages during metamorphism, differences that may have affected the distribution and modal abundance of epidote among analyzed samples. In order to further analyze this effect, we retain reference to bulk-composition subgroups A and B throughout this paper.

## REE Distribution Coefficients

Numerous investigators (*e.g.*, Kretz, 1959, 1961, Sorensen & Grossman 1989, Hickmott & Spear 1992, Dahl *et al.* 1993, Kretz *et al*. 1999, Pyle & Spear 1999, 2000, Yang *et al.* 1999, Yang & Rivers 2000, Skublov & Drugova 2003) have attempted to model trace-element variations in natural metamorphic systems using distribution coefficients. In this study, the distributions of the REE between two coexisting phases A and B are defined using the Nielsen (1985) distribution coefficient, $D^*_{REE} = X_{REE}^{A} / X_{REE}^{B}$, where $X_{REE}$ is the mole fraction of the REE in specific crystallographic sites in minerals A and B. Values of $D^*_{REE}$ for representative pairs of minerals in the four samples are listed in Table 4; we assume that the REE enter the 8-fold-coordinated *M*4 (Ca) site in Ca amphibole, the 7- to 9-fold coordinated *A* site in plagioclase, and the 8- and 7-fold coordinated Ca sites in epidote and titanite, respectively, based on considerations of ionic radii and site size (Shannon 1976, Smith & Brown 1987, Smyth & Bish 1988). $D^*_{REE}$ values are plotted against ionic radius in Onuma-type diagrams (Onuma *et al*. 1968, Jensen 1973, Yang *et al.* 1999) illustrated in Figure 8. Analytical uncertainties in this figure are given as 1σ standard deviation measured from LAM–ICP–MS counting statistics.

In Onuma-type diagrams for *Ca amphibole–titanite* pairs (Fig. 8a), LREE, MREE, and HREE all preferentially partition into titanite, but two patterns are present that appear to be linked to bulk-rock composition, *i.e.*, subgroups A and B (neglecting sample 06 because of its atypical chondrite-normalized REE pattern for titanite). Patterns of $D^*_{REE}{}^{Amp/Ttn}$ for samples 46 and 48 (subgroup A) exhibit a downward slope toward the LREE and partition coefficients between 0.01 and 0.001, whereas sample 49 (subgroup B) exhibits a much flatter pattern with a partition coefficient of ~0.1. We infer that the change in slope and approximately order-of-magnitude increase in the value of the partition coefficients in subgroup B relates to the lower cummingtonite content of the amphibole. Patterns for *Ca amphibole–plagioclase* pairs (Fig.8b) show that most REE, especially the MREE and HREE, preferentially partition into the Ca amphibole. However, there is a significant variation in the magnitude of REE partition coefficients that we attribute to changes in major-element composition of each phase (discussed further below). Patterns for *Ca amphibole–epidote* pairs (Fig. 8c) show that the LREE preferentially partition into epidote, whereas the HREE partition into Ca amphibole. In addition, there is a small increase in the magnitude of $D^*_{REE}{}^{Amp/Ep}$ for sample 06 that we infer is linked to decreasing $X_{Cum}{}^{Amp}$.

In *titanite–plagioclase* pairs (Fig. 8d), all the REE preferentially partition into titanite, but REE partitioning appears to be sensitive to plagioclase composition. For instance, there is a decrease in $D^*_{LREE}{}^{Ttn/Pl}$ of approximately an order of magnitude between samples in subgroups B and A, which we infer is related to the increase in $X_{An}{}^{Pl}$. All the REE preferentially partition into titanite between *titanite–epidote* pairs (Fig. 8e), with titanite exhibiting a stronger preference for MREE and HREE relative to the LREE. All REE preferentially partition into epidote in *plagioclase–epidote* pairs (Fig. 8f), but the distribution pattern of the HREE is erratic, reflecting the low abundances of HREE in plagioclase. As in several other mineral pairs, there is a significant change in $D^*_{Eu}{}^{Pl/Ep}$ compared to the adjacent REE, compatible with the presence of Eu in $Eu^{3+}$ and $Eu^{2+}$ states.

## Controls on Incorporation of the Rare-Earth Elements

### *Thermodynamic background*

The thermodynamic basis for the distribution of a trace element between a pair of coexisting minerals can be viewed in terms of an exchange reaction with a major element, for which the thermodynamic principles are well established (*e.g.*, Kretz 1959, 1961). These principles are summarized by Yang *et al*. (1999). Despite the possibility of strong interactions of trace elements with adjacent ions in the structure, activity–composition (*a–X*) relationships remain relatively simple owing to

the intrinsically low concentrations of trace elements, which do not affect the average structural environment of the mineral. Compositional and crystal-structure effects on REE partitioning are discussed below.

*Compositional effects*

A useful way to examine the compositional dependency of the REE partitioning is to compare it with the concentration of a major element that occupies the same site in one or both of the minerals. For instance, Yang *et al.* (1999) and Yang & Rivers (2000) employed this approach to investigate the major-element compositional controls of garnet, biotite, and muscovite on trace-element partitioning in garnet–biotite and biotite–muscovite pairs. In this study, we compare ΣREE and selected ratios of LREE, MREE, and HREE to appropriate exchange-vectors and molar fractions in Ca amphibole, plagioclase, epidote, and titanite.

The REE are generally considered to enter the large *M*4 site in *Ca amphibole* by a coupled substitution such

TABLE 4. AVERAGE VALUES ($n$ = 3) OF $D^*_{REE}{}^{MIN1/MIN2}$ FOR PAIRS OF ANALYZED MINERALS IN METABASIC ROCKS FROM THE ST. ANTHONY COMPLEX, NEWFOUNDLAND

| $D^{*AMP/TTN}$ | 46 | SD | 48 | SD | 06 | SD | 49 | SD |
|---|---|---|---|---|---|---|---|---|
| La | 0.01 | 4.0E-03 | 2.0E-3 | 7.8E-04 | 0.04 | 2.0E-02 | 0.102 | 2.2E-02 |
| Ce | 0.01 | 3.7E-03 | 2.0E-3 | 6.3E-04 | 0.04 | 1.5E-02 | 0.09 | 1.6E-02 |
| Pr | 0.01 | 5.0E-03 | 3.0E-3 | 8.9E-04 | 0.05 | 2.3E-02 | 0.09 | 1.6E-02 |
| Nd | 0.01 | 4.2E-03 | 4.0E-3 | 6.5E-04 | 0.06 | 2.2E-02 | 0.09 | 1.6E-02 |
| Sm | 0.02 | 4.5E-03 | 0.01 | 1.2E-03 | 0.09 | 4.3E-02 | 0.08 | 1.1E-02 |
| Eu | 0.02 | 5.8E-03 | 0.01 | 4.5E-04 | 0.08 | 3.1E-02 | 0.08 | 1.1E-02 |
| Gd | 0.02 | 3.1E-03 | 0.01 | 1.4E-03 | 0.18 | 9.0E-02 | 0.08 | 1.2E-02 |
| Tb | 0.02 | 1.5E-03 | 0.01 | 1.4E-03 | 0.28 | 1.5E-01 | 0.08 | 1.2E-02 |
| Dy | 0.02 | 1.2E-03 | 0.01 | 2.2E-03 | 0.37 | 2.1E-01 | 0.07 | 1.1E-02 |
| Ho | 0.02 | 2.9E-03 | 0.02 | 2.0E-03 | 0.67 | 3.7E-01 | 0.08 | 1.1E-02 |
| Er | 0.03 | 9.9E-04 | 0.02 | 1.8E-03 | 1.02 | 5.7E-01 | 0.08 | 1.1E-02 |
| Tm | 0.03 | 3.3E-03 | 0.02 | 2.6E-03 | 1.24 | 7.2E-01 | 0.08 | 1.2E-02 |
| Yb | 0.03 | 1.9E-03 | 0.02 | 2.2E-03 | 2.03 | 1.2E+00 | 0.09 | 1.2E-02 |
| Lu | 0.04 | 6.6E-03 | 0.02 | 2.1E-03 | 2.02 | 1.3E+00 | 0.11 | 1.5E-02 |

| $D^{*AMP/PL}$ | 46 | SD | 48 | SD | 06 | SD | 49 | SD |
|---|---|---|---|---|---|---|---|---|
| La | 1.34 | 8.7E-01 | 0.29 | 0.10 | 1.24 | 1.00 | 3.28 | 0.20 |
| Ce | 5.36 | 1.50 | 1.03 | 0.10 | 2.78 | 1.60 | 11.02 | 0.40 |
| Pr | 10.21 | 2.20 | 1.13 | 1.00 | 7.46 | 3.00 | 22.45 | 1.00 |
| Nd | 21.39 | 9.30 | 1.92 | 0.40 | 17.50 | 6.10 | 41.51 | 0.70 |
| Sm | 30.95 | 6.50 | 3.92 | 0.50 | 37.42 | 8.60 | 105.8 | 7.80 |
| Eu | 4.40 | 2.40 | 0.15 | 0.00 | 13.83 | 2.70 | 21.52 | 5.20 |
| Gd | 44.93 | 7.70 | 6.67 | 3.70 | 73.80 | 7.50 | 338.5 | 24.50 |
| Tb | 136.0 | | 6.59 | 0.40 | 91.74 | 12.30 | 279.8 | 57.10 |
| Dy | 151.6 | 121.9 | 12.61 | 2.70 | 62.27 | 3.80 | 478.0 | 50.00 |
| Ho | | | 11.65 | 4.60 | 100.1 | 7.60 | 430.6 | 7.90 |
| Er | 102.6 | 49.80 | 14.86 | 4.40 | 136.7 | 25.90 | 267.8 | 6.70 |
| Tm | 68.06 | | 9.56 | 4.10 | 61.73 | 18.40 | 148.0 | 32.40 |
| Yb | 68.28 | 40.0 | 15.34 | 2.00 | 65.98 | 19.80 | 292.0 | 44.00 |
| Lu | | | 11.29 | | 90.74 | | 263.3 | |

| $D^{*AMP/EP}$ | 46 | SD | 48 | SD | 06 | SD |
|---|---|---|---|---|---|---|
| La | 0.01 | 1.8E-02 | 0.02 | 2.2E-03 | 0.07 | 2.6E-02 |
| Ce | 0.03 | 5.5E-02 | 0.03 | 6.2E-03 | 0.14 | 4.8E-02 |
| Pr | 0.05 | 7.6E-02 | 0.06 | 1.1E-02 | 0.24 | 9.8E-02 |
| Nd | 0.08 | 8.5E-02 | 0.10 | 2.3E-02 | 0.38 | 1.1E-01 |
| Sm | 0.19 | 1.7E-01 | 0.25 | 5.3E-02 | 0.73 | 2.0E-01 |
| Eu | 0.18 | 2.4E-01 | 0.19 | 3.7E-02 | 0.73 | 1.6E-01 |
| Gd | 0.42 | 4.1E-01 | 0.59 | 1.0E-01 | 1.30 | 3.5E-01 |
| Tb | 0.53 | 3.8E-01 | 0.75 | 1.0E-01 | 1.68 | 3.6E-01 |
| Dy | 0.76 | 4.9E-01 | 0.94 | 1.4E-01 | 2.02 | 4.1E-01 |
| Ho | 0.93 | 4.7E-01 | 1.18 | 1.5E-01 | 2.42 | 5.3E-01 |
| Er | 1.08 | 5.1E-01 | 1.28 | 1.5E-01 | 3.03 | 9.2E-01 |
| Tm | 1.23 | 5.7E-01 | 1.47 | 1.9E-01 | 3.54 | 1.80 |
| Yb | 1.34 | 1.8E-01 | 1.42 | 2.6E-01 | 3.87 | 2.30 |
| Lu | 1.52 | 1.8E-01 | 1.77 | 3.3E-01 | 4.31 | 2.10 |

| $D^{*TTN/PL}$ | 46 | SD | 48 | SD | 06 | SD | 49 | SD |
|---|---|---|---|---|---|---|---|---|
| La | 353.3 | 74.00 | 210.4 | 106.9 | 39.05 | 1.50 | 25.71 | 12.00 |
| Ce | 821.3 | 281.4 | 455.2 | 136.4 | 78.34 | 0.60 | 98.41 | 36.90 |
| Pr | 1240 | 435.0 | 340.6 | 41.80 | 191.9 | 6.60 | 206.5 | 49.40 |
| Nd | 2170 | 831.0 | 466.9 | 205.1 | 410.4 | 14.70 | 410.7 | 107.7 |
| Sm | 2258 | 303.6 | 516.7 | 96.80 | 782.7 | 53.90 | 1143 | 348.3 |
| Eu | 327.5 | 274.5 | 26.23 | 8.20 | 241.2 | 12.80 | 209.7 | 134.2 |
| Gd | 2609 | 372.1 | 620.7 | 232.3 | 1141 | 118.4 | 3586 | 738.8 |
| Tb | 7925 | | 537.7 | 81.90 | 1103 | 230.9 | 2889 | 1439 |
| Dy | 7129 | 5622 | 994.9 | 176.8 | 584.5 | 120.9 | 5230 | 2055 |
| Ho | | | 758.2 | 201.6 | 586.3 | 172.7 | 4398 | 1146 |
| Er | 4213 | 1412 | 957.9 | 367.9 | 519.2 | 83.00 | 2729 | 753.3 |
| Tm | 2733 | | 571.3 | 130.4 | 162.0 | 16.90 | 1492 | 720.3 |
| Yb | 2506 | 293.0 | 893.5 | 268.2 | 115.2 | 29.60 | 2833 | 313.8 |
| Lu | | | 303.0 | 191.0 | 817.7 | 6.30 | 2106 | 400.9 |

| $D^{*TTN/EP}$ | 46 | SD | 48 | SD | 06 | SD |
|---|---|---|---|---|---|---|
| La | 3.02 | 1.00 | 13.22 | 2.60 | 2.29 | 0.40 |
| Ce | 4.94 | 0.60 | 14.82 | 2.40 | 3.97 | 0.30 |
| Pr | 5.75 | 0.80 | 19.34 | 1.30 | 6.07 | 0.50 |
| Nd | 7.61 | 0.70 | 24.62 | 0.90 | 8.83 | 0.70 |
| Sm | 13.50 | 0.30 | 32.78 | 0.20 | 15.23 | 0.20 |
| Eu | 13.52 | 1.40 | 34.33 | 0.80 | 12.80 | 1.50 |
| Gd | 24.33 | 1.00 | 55.08 | 3.50 | 20.05 | 0.40 |
| Tb | 30.93 | 0.10 | 60.82 | 4.40 | 20.21 | 0.00 |
| Dy | 35.78 | 1.50 | 74.38 | 4.10 | 18.94 | 0.40 |
| Ho | 40.34 | 0.50 | 76.94 | 4.10 | 14.18 | 0.10 |
| Er | 44.35 | 1.50 | 82.39 | 5.40 | 11.51 | 0.00 |
| Tm | 49.26 | 6.00 | 87.89 | 9.40 | 9.30 | 0.10 |
| Yb | 49.22 | 3.10 | 82.52 | 7.10 | 6.75 | 0.00 |
| Lu | 46.69 | 2.10 | 47.55 | 3.40 | 38.86 | 3.30 |

| $D^{*PL/EP}$ | 46 | SD | 48 | SD | 06 | SD |
|---|---|---|---|---|---|---|
| La | 0.01 | 2.1E-03 | 1.54E-04 | 3.0E-03 | 0.06 | 7.5E-03 |
| Ce | 0.01 | 1.4E-03 | 4.55E-04 | 2.4E-03 | 0.05 | 6.6E-03 |
| Pr | | 1.1E-03 | 5.93E-05 | 8.9E-02 | 0.03 | 8.8E-03 |
| Nd | | 1.8E-03 | 2.49E-04 | 1.1E-02 | 0.02 | 4.4E-03 |
| Sm | 0.01 | 5.6E-05 | 5.67E-05 | 3.7E-02 | 0.02 | 4.4E-03 |
| Eu | 0.04 | 1.5E-02 | 1.92E-05 | 8.6E-01 | 0.05 | 1.1E-02 |
| Gd | 0.01 | 1.2E-03 | 4.01E-05 | 1.2E-01 | 0.02 | 7.1E-03 |
| Tb | | | 5.76E-06 | 5.9E-02 | 0.02 | 9.3E-03 |
| Dy | 0.01 | 2.8E-03 | 3.28E-05 | 2.8E-02 | 0.03 | 1.2E-02 |
| Ho | | | 6.09E-06 | 9.7E-02 | 0.02 | 1.0E-02 |
| Er | 0.01 | 6.6E-05 | 1.62E-05 | 6.5E-02 | 0.02 | 6.8E-03 |
| Tm | 0.02 | 1.5E-02 | 2.11E-06 | 2.0E-01 | 0.06 | 1.4E-02 |
| Yb | 0.02 | 1.8E-02 | 1.50E-05 | 1.6E-01 | 0.06 | 1.2E-02 |
| Lu | | | 2.17E-06 | | 0.05 | |

SD is the standard deviation at one sigma. The absence of a standard deviation represents a single determination. Blank indicates below detection limits for one phase.

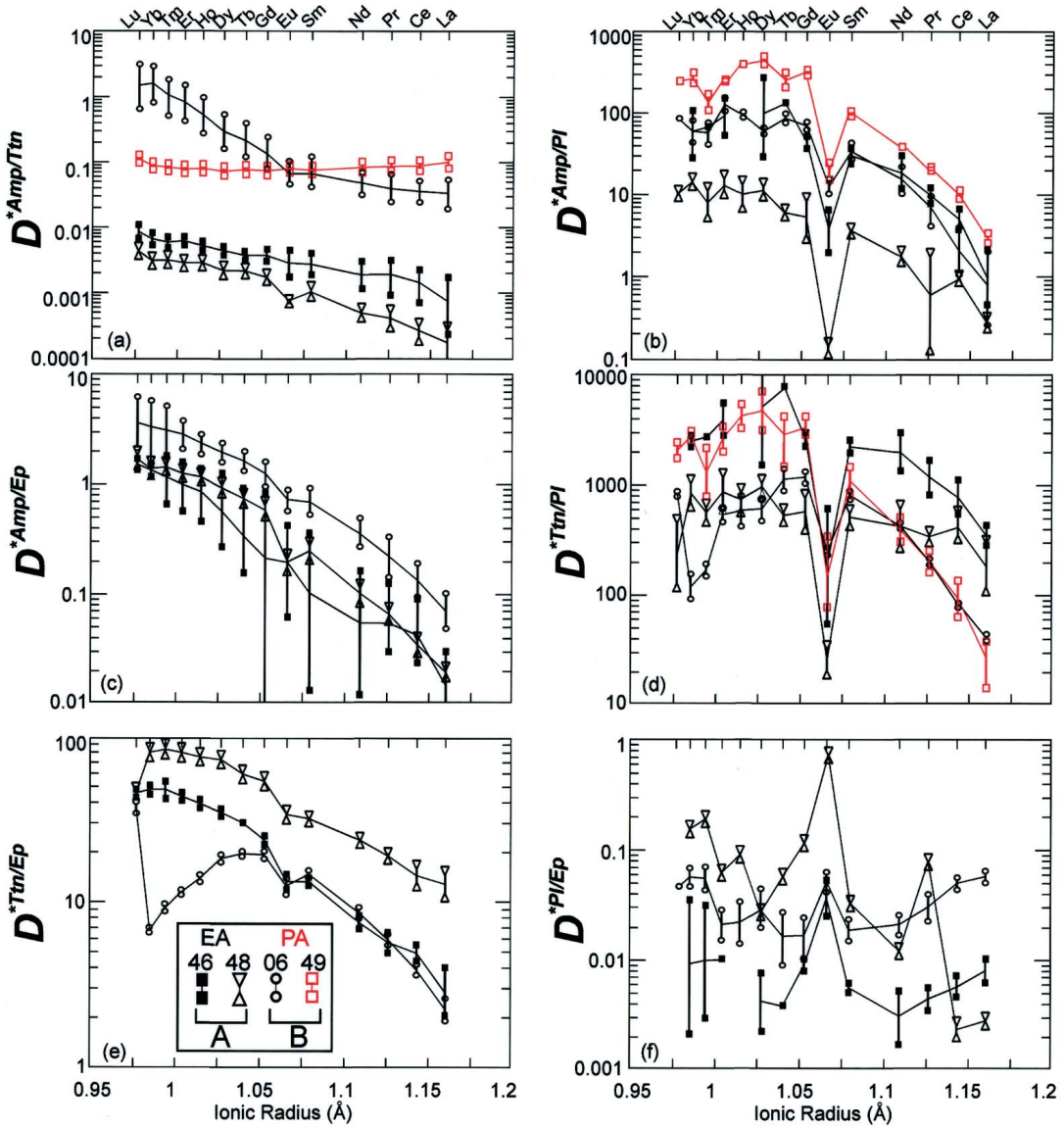


FIG. 8. $D^*_{REE}$ distribution coefficients for six pairs of minerals. Error bars represent one standard deviation. EA: epidote amphibolite, PA: plagioclase amphibolite; A and B refer to bulk-composition subgroups defined in the text and in Figure 3a.

as: $^{M4}Ca^{2+} + {}^{IV}Si^{4+} \leftrightarrow {}^{M4}REE^{3+} + {}^{IV}Al^{3+}$. However, Figure 9a illustrates the positive correlation (r' = 0.67) between $X_{Cum}^{Amp}$ and the ratio of Σ(HREE + MREE)/LREE in the Ca amphibole analyzed. This relationship, first described by Bottazzi *et al.* (1999) for kaersutitic amphibole with a significant cummingtonite component, suggests that the REE may partition at two *M*4 sites in the Ca amphibole structure (*M*4 and *M*4'), as discussed in more detail below. In analyzed *plagioclase*, there is a broad positive correlation (r' = 0.66) between $X_{An}^{Pl}$ and the ratio Σ(LREE + MREE)/(HREE) (Fig. 9b), which is attributed to the structural constriction of the 7- to 9-fold coordinated *A* site in plagioclase with increasing calcium content, such that the cavity becomes closer to the ionic radii of LREE. It is well established that plagioclase incorporates more LREE relative to HREE, a feature also exemplified by the data in this study (Table 2, Fig. 5b). However, if only plagioclase

coexisting with epidote is considered (*i.e.*, omitting sample 49), the correlation is stronger ($r'^{E} = 0.73$) and clearly related to modal % epidote, suggesting that the correlation is a result of the net transfer of Ca and REE from epidote to plagioclase during epidote breakdown. The incorporation of the REE in plagioclase may be charged-balanced by a coupled substitution involving Al, Na and a pentavalent species such as P; *e.g.*, $^{A}Na^{1+} + {}^{T}P^{5+} \leftrightarrow {}^{A}REE^{3+} + {}^{T}Al^{3+}$.

There is a broad positive correlation between Al content ($X_{Czo}^{Ep}$) and ΣREE in the *epidote* analyzed (Fig. 9c). However, within-sample variations in total REE abundance are significant and likely related to within- and between-grain zoning (Fig. 2d). On the basis of ionic radii (Smyth & Bish 1988), all REE are considered to substitute at the *X* site in epidote, normally occupied by calcium. To preserve electroneutrality, REE incorporation must be coupled with substitution of a divalent cation in octahedral *M*3 sites, *e.g.*, $^{X}Ca^{2+} + {}^{M3}Al^{3+} \leftrightarrow {}^{X}REE^{3+} + {}^{M3}(Fe,Mg)^{2+}$.

Deer *et al.* (1966) and Green & Pearson (1986) proposed a mechanism involving REE substitution for calcium in the 7-fold coordinated *X* sites of *titanite*, with charge balance achieved by $(Al,Fe^{3+})$ substitution for Ti at octahedral sites, *i.e.*, $Ca^{2+} + Ti^{4+} \leftrightarrow REE^{3+} + Al^{3+}$. Data published by Tiepolo *et al.* (2002) for synthetic titanite have confirmed this exchange mechanism, but no correlations between ΣREE or a ratio of REE and major components in titanite were discovered in our samples, possibly due to the restricted compositional range in terms of major elements.

There are thus correlations between major-element composition, ΣREE and selected ratios of LREE, MREE and HREE in three of the four phases examined, implying that compositional controls on REE incorporation are likely a significant factor in the measured distributions.

### *Crystal-structure effects*

The first-order constraints imposed by the crystal structure on trace-element partitioning are the charge and ionic radius of the trace element in relation to the nominal charge and volume of the host polyhedron (*e.g.*, Onuma *et al.* 1968, Brice 1975, Blundy & Wood 1994). A second-order constraint is the elasticity of the structure, *i.e.*, relatively elastic structures will admit misfitting ions or coupled substitutions more readily than those that are more rigid by permitting structural distortions to accommodate local changes in ion size and charge. However, it is debatable whether the results in this study can be explained in terms of variations in elas-

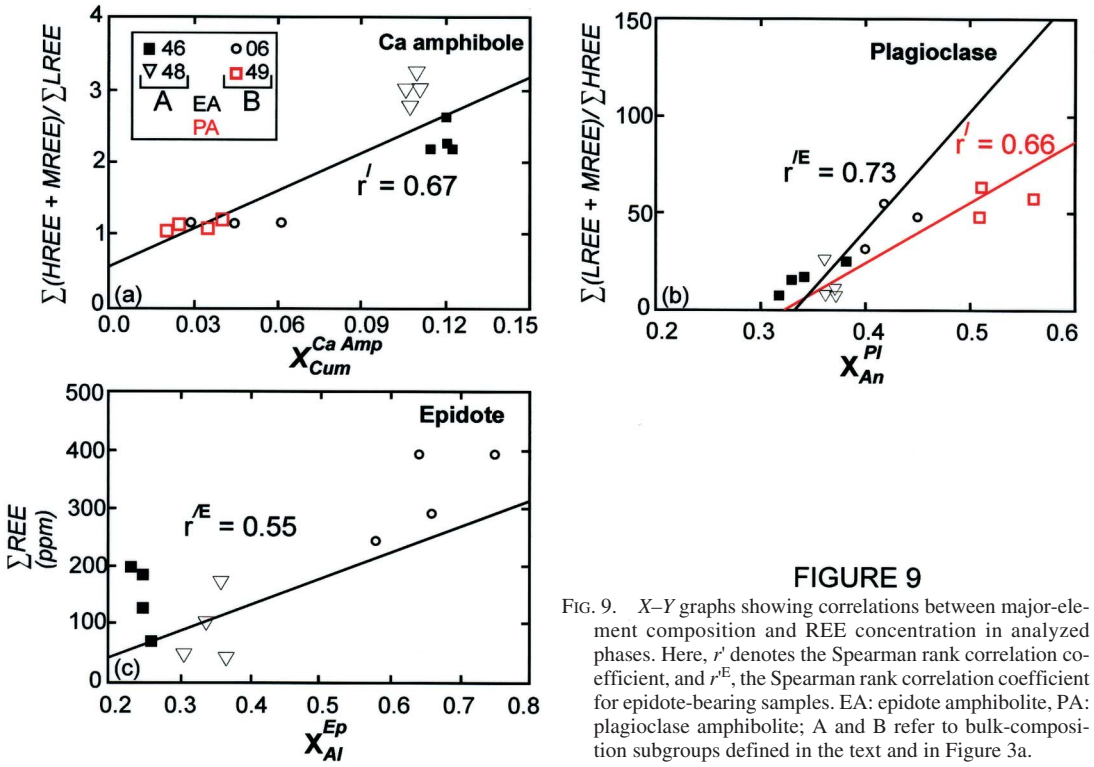


FIGURE 9

FIG. 9. *X–Y* graphs showing correlations between major-element composition and REE concentration in analyzed phases. Here, *r'* denotes the Spearman rank correlation coefficient, and $r'^{E}$, the Spearman rank correlation coefficient for epidote-bearing samples. EA: epidote amphibolite, PA: plagioclase amphibolite; A and B refer to bulk-composition subgroups defined in the text and in Figure 3a.

ticity because of the limited *P–T* range of the samples analyzed.

The Onuma-type diagrams in Figure 8 reflect the combined effects of the sites in both minerals on which partitioning occurs. Their shapes depend on the partitioning behavior of each phase in a given pair of minerals, which in turn is influenced by site characteristics, major-element composition, and valence state of substituting cation, for example, rendering quantitative extraction of the ideal site-sizes and elasticities using the equation of Blundy & Wood (1994) impractical in many cases. Considering only the effects of elasticity of the structure and optimal radius ($r_o$), and ignoring local charge-balance effects due to potential coupled substitutions, Figure 10 schematically illustrates possible scenarios for the shapes of Onuma-type diagrams based on mineral pairs with various site-characteristics. Since there is an almost infinite range of possibilities for the shapes of these curves, Figure 10 is only a simplified illustration. In the case of a crystal/liquid pair (Fig. 10a; Onuma's case), liquid has negligible influence on the shape of the Onuma curve since its structure is much more elastic than that of the coexisting mineral, and the vertex of the parabola therefore represents the ideal ra-

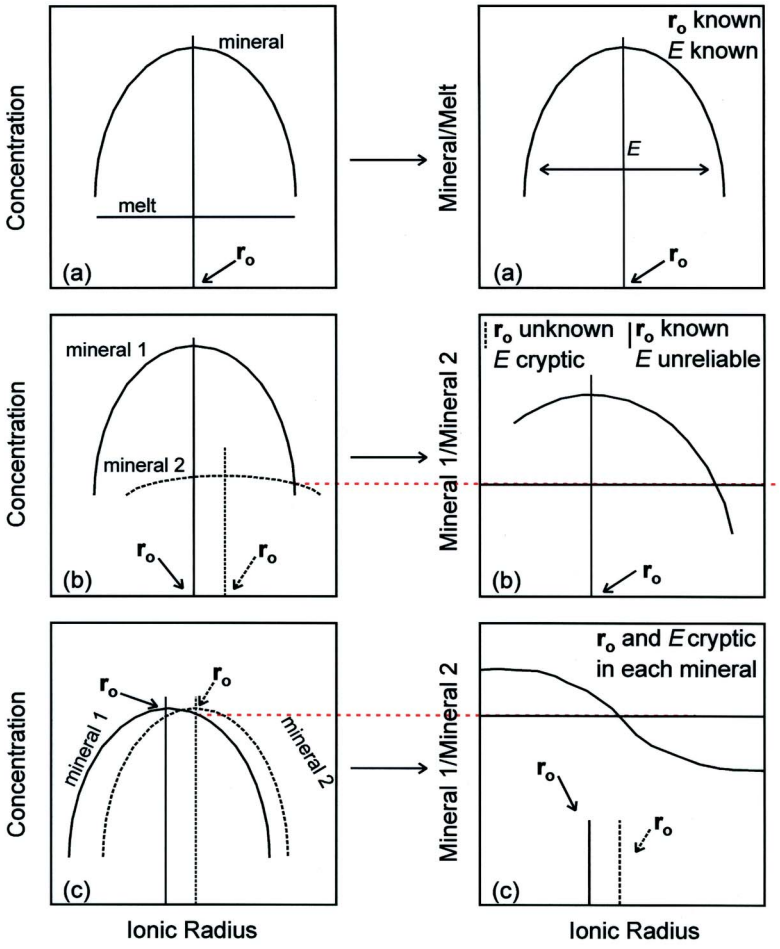


FIG. 10. Schematic Onuma $D^*_{REE}{}^{Mineral/Liquid}$ and Onuma-type $D^*_{REE}{}^{Min1/Min2}$ curves: a) $D^*_{REE}{}^{Mineral/Liquid}$ curve, in which the shape of the parabola is entirely controlled by the site in the mineral. (b) $D^*_{REE}{}^{Min1/Min2}$ curve showing an example of sites in two minerals with very different elasticities, but similar ionic radii; c) $D^*_{REE}{}^{Min1/Min2}$ curve showing an example of sites in two minerals with similar ionic radii and elasticities. Here, $r_0$ is the ideal ionic radius for the site, $E$ is the elasticity. Dashed red line indicates equal partitioning between the two phases. After P. Yang (pers. commun., 2003).

dius of the site in the mineral on which substitution occurs, with the convexity reflecting its elasticity. In the case of mineral–mineral partitioning (Figs. 10b–c), trace element *i* is partitioned between two minerals with distinct polyhedra (*i.e.*, with differences in $r_o$ or elasticity or both). In Figure 10b, the Onuma-type diagram is similar to a crystal–liquid Onuma diagram since control on partitioning is dominated by one of the two phases [*e.g.*, HREE partitioning in garnet–biotite pairs controlled by garnet *X* sites: Yang *et al.* (1999); LILE and HFSE partitioning in Ca-amphibole–clinopyroxene pairs dominated by $^{XII}A$ and $^{VI}M$ sites in Ca amphibole, respectively: Tiepolo *et al.* (2000)]. In principle, in cases such as these, the ideal ionic radius of the site in the "dominant" mineral may be approximated from such a diagram, but the ideal ionic radius of the site in the "subordinate" mineral is cryptic. Figure 10c illustrates cation partitioning between two minerals with analogous polyhedra that exhibit only slight differences in size and elasticity. In this case, the shape of the Onuma-type curve reflects the combined effects of the two sites (one or possibly more in each mineral), and their ideal ionic radii and elasticities in both phases are cryptic (*e.g.*, epidote *X* and titanite *A* sites; Fig. 8e, this study). Because of these problems, in this study we have developed a qualitative approach to the extraction of site parameters in the two minerals that nonetheless provides significant insight into partitioning behavior. We use representative Onuma-type curves for the six pairs of minerals (solid black lines in Fig. 11) to infer qualitative information concerning the sizes and elasticities of the sites in each mineral on which REE substitution occurs (shown as dashed lines).

Onuma-type curves for *amphibole–titanite* pairs are of two types, those for subgroup A, sloping monotonically with a peak near the HREE (Fig. 11a), and those for subgroup B, which are approximately flat (Fig. 11b). Owing to the limited major-element compositional variability and the internally coherent, relatively unfractionated, chondrite-normalized REE patterns exhibited by titanite (Fig. 6d), we attribute the different shapes of the two plots principally to Ca amphibole (Fig. 6a). The two patterns correlate with the amount of cummingtonite component in solid solution, *i.e.*, those for subgroup A ($X_{Cum}^{Amp} \approx 0.12$) rise to a maximum value at Lu, whereas those for subgroup B ($X_{Cum}^{Amp} \approx 0.03$) are much flatter. Bottazzi *et al.* (1999) were the first to suggest a correlation between REE uptake in Ca amphibole and $X_{Cum}^{Amp}$. On the basis of their kaersutite–liquid and pargasite–liquid experimental data, they proposed a two-site model of REE incorporation in Ca amphibole, with the larger LREE being preferentially incorporated at the *M*4 (Ca) site, and the smaller HREE on the *M*4' (Fe,Mg) site. They determined the ideal radii of the *M*4 and *M*4' sites in the two types of Ca amphibole by structure refinement, and we qualitatively follow their model in interpreting our data (Figs. 11a–b). The representative Onuma-type pattern for *titanite–plagioclase* pairs (Fig. 11c) displays an irregular quasi-parabolic shape with a minimum in the LREE range (≈ La, ≈1.16 Å) and a peak in the MREE range at Tb (≈1.06 Å). We attribute these features to the preference of LREE for the plagioclase *A* site and to a single elastic *A* site in titanite with a vertex in the MREE range that dominates the incorporation of all the REE.

Onuma-type plots for *Ca amphibole – plagioclase* pairs (Fig. 11d) are similar to those for titanite–plagioclase pairs, implying that Ca amphibole *M*4 sites, especially those with limited cummingtonite exchange (*i.e.*, samples 06 and 49), dominate over plagioclase *A* sites as hosts for all REE except La, which is approximately equally distributed between the two phases. Onuma-type diagrams for *titanite–epidote* pairs for samples 46 and 48 (Fig. 8e) display monotonic slopes with minima near La and maxima near Lu that are interpreted to be a result of single elastic sites in titanite (*A* site) and epidote (*X* site) with vertices near Sm and La, respectively (Fig. 11e).

We conclude from these plots that the proposed site-distribution models for epidote, plagioclase, titanite and amphibole are qualitatively viable, justifying their application to the remaining *plagioclase–epidote* and *amphibole–epidote* pairs (Figs.11f–g), which also yield internally consistent results. For instance, all $D^*_{REE}^{Pl/Min}$ and $D^*_{REE}^{Ep/Min}$ pairs require a single-site model with a major peak in the LREE for plagioclase and epidote, all $D^*_{REE}^{Ttn/Min}$ pairs can be reconciled with a single-site elastic model with a peak in the MREE range for this phase, and Ca amphibole requires a two-site model with variable development of the *M*4' peak depending on the value of $X_{Cum}^{Amp}$.

## Mass Balance of the Rare-Earth Elements

### *Background*

Mass-balance calculations have been used previously to determine the roles of specific phases as reservoirs or carriers for certain trace elements in metamorphic rocks (*e.g.*, Sorensen & Grossman 1989, Tribuzio *et al.* 1996, Nagasaki & Enami 1998, Zack *et al.* 2002). Such calculations require knowledge of both

FIG. 11. $D^*_{REE}^{Min1/Min2}$ Onuma-type diagrams for the six pairs of minerals examined in this study (solid black lines) and inferred $r_0$ values and elasticities of sites in the two minerals at which the REE substitute (dashed lines: blue: Ca amphibole, brown: titanite, green: epidote, purple: plagioclase). Two pairs of diagrams are included for Ca amphibole–titanite because of contrasting behavior of *M*4 and *M*4' sites in "cummingtonite-rich" and "cummingtonite-poor" amphibole.

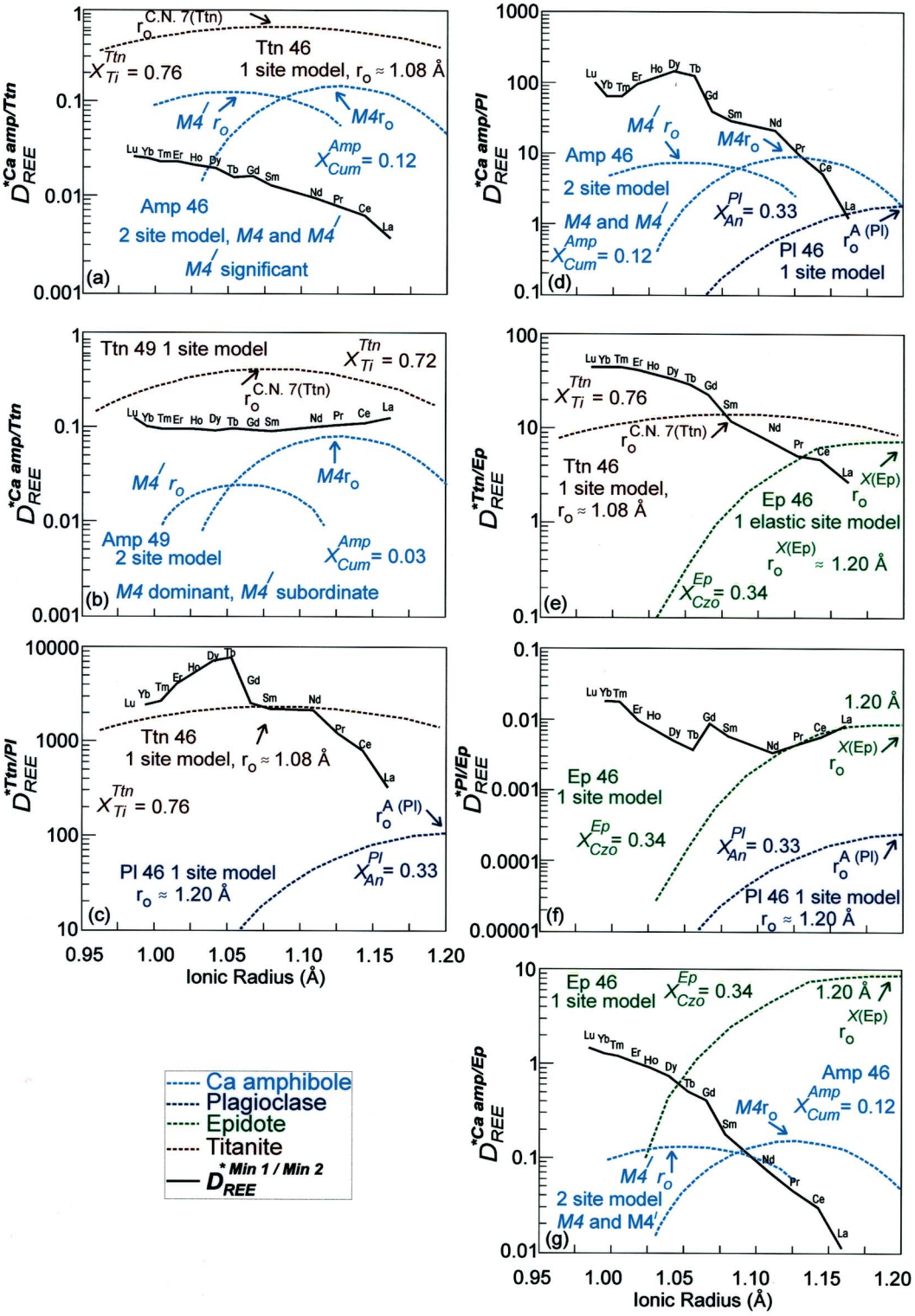
(a)
C.N. 7(Ttn)
Ttn 46
1 site model, r_o ≈ 1.08 Å
X_Ti^Ttn = 0.76
M4 r_o
M4r_o
X_Cum^Amp = 0.12
Amp 46
2 site model, M4 and M4'
M4' significant
*Ca amp/Ttn D_REE
(b)
Ttn 49 1 site model
X_Ti^Ttn = 0.72
C.N. 7(Ttn)
M4 r_o
M4r_o
Amp 49
2 site model
X_Cum^Amp = 0.03
M4 dominant, M4' subordinate
*Ca amp/Ttn D_REE
(c)
Ttn 46
1 site model, r_o ≈ 1.08 Å
X_Ti^Ttn = 0.76
r_o^A (Pl)
PI 46 1 site model
r_o ≈ 1.20 Å
X_An^Pl = 0.33
*Ttn/Pl D_REE
Ionic Radius (Å)
(d)
M4 r_o
M4r_o
Amp 46
2 site model
M4 and M4'
X_Cum^Amp = 0.12
X_An^Pl = 0.33
PI 46
1 site model
r_o^A (Pl)
*Ca amp/Pl D_REE
(e)
X_Ti^Ttn = 0.76
C.N. 7(Ttn)
Ttn 46
1 site model,
r_o ≈ 1.08 Å
Ep 46
1 elastic site model
X(Ep) r_o ≈ 1.20 Å
X_Czo^Ep = 0.34
*Ttn/Ep D_REE
(f)
1.20 Å
X(Ep) r_o
Ep 46
1 site model
X_Czo^Ep = 0.34
X_An^Pl = 0.33
r_o^A (Pl)
PI 46 1 site model
r_o ≈ 1.20 Å
*Pl/Ep D_REE
(g)
Ep 46
1 site model
X_Czo^Ep = 0.34
1.20 Å
X(Ep) r_o
Amp 46
X_Cum^Amp = 0.12
M4r_o
M4 r_o
2 site model
M4 and M4'
*Ca amp/Ep D_REE
Ionic Radius (Å)
Ca amphibole
Plagioclase
Epidote
Titanite
*Min 1 / Min 2 D_REE

the concentrations and modal abundances of all coexisting phases to calculate a reconstructed whole-rock concentration. The results are then compared with the measured whole-rock trace-element concentrations in the same samples, which serve as an independent control on quality. Here, we use modal estimates and abundances of the REE in minerals representative of equilibrium assemblages to perform mass balances for REE on the same four samples (46 and 48, subgroup A; 06 and 49, subgroup B) in order to evaluate the relative importance of individual minerals as carriers of the REE in epidote amphibolite and plagioclase amphibolite. Values from representative assemblages within each thin section were used rather than average values for the whole thin section, so that the results would not be skewed by strongly zoned grains.

*Mass balance: results*

Results and error estimates for subgroup A (epidote amphibolite: samples 46 and 48), presented in Table 5 and illustrated in Figures 12a–b, are very similar and are addressed together. Absolute errors in REE budgets are small and all, except for Ho in sample 48, are within 20% of the measured whole-rock values. Despite a modal abundance of approximately 2%, titanite is the principal carrier (50–80%) of all REE. Epidote is an important LREE sink (10 to 15%), and Ca amphibole, the most voluminous phase, sequesters approximately 5 to 30% of the REE, with a progressive increase from LREE to HREE. Plagioclase (15–18 modal %) accounts for minor (<5%) amounts of LREE and variable amounts (up to 15%) of Eu, but is otherwise an insignificant carrier of REE.

Results and error estimates for subgroup B (06: epidote amphibolite, 49: plagioclase amphibolite) are presented in Table 5 and illustrated in Figures 12c–d. They point to a major redistribution of the REE among the coexisting phases. The fits between the REE budgets and measured bulk-rock abundances for the LREE are not as good than those for the previous samples, but most HREE and LREE budgets are within approximately 10 and 30%, respectively, of the measured whole-rock abundances. In the epidote amphibolite (sample 06), Ca amphibole carries 30–90% of the REE budget, favoring the MREE and HREE, and epidote carries 10–30% of the LREE. Titanite, the dominant REE sink in subgroup-A samples, accounts for only 5–

TABLE 5. REE MASS-BALANCE DATA

| Sample 46 | Amp | Ep | Pl | Ttn | Total | Meas. | %Diff. |
|---|---|---|---|---|---|---|---|
| Mode % | 65 | 10 | 18 | 2 | | (+ 5% Quartz) | |
| | | Epidote amphibolite: reconstructed REE | | | | | |
| La ppm | 0.14 | 0.87 | 0.02 | 3.40 | 4.44 | 5.26 | –16 |
| Ce | 0.85 | 1.71 | 0.03 | 11.06 | 13.66 | 15.65 | –13 |
| Pr | 0.15 | 0.22 | | 1.75 | 2.13 | 2.31 | –8 |
| Nd | 0.92 | 1.10 | 0.01 | 9.20 | 11.23 | 12.24 | –8 |
| Sm | 0.41 | 0.24 | | 2.90 | 3.55 | 4.28 | –17 |
| Eu | 0.13 | 0.50 | 0.02 | 0.79 | 1.45 | 1.55 | –7 |
| Gd | 0.61 | 0.93 | 0.01 | 3.04 | 4.59 | 5.84 | –21 |
| Tb | 0.15 | 0.04 | | 0.63 | 0.81 | 1.00 | –18 |
| Dy | 1.29 | 0.23 | | 4.34 | 5.86 | 6.71 | –13 |
| Ho | 0.23 | 0.07 | | 0.62 | 0.92 | 1.34 | –31 |
| Er | 0.94 | 0.14 | | 2.60 | 3.68 | 3.91 | –6 |
| Tm | 0.15 | 0.02 | | 0.37 | 0.54 | 0.57 | +5 |
| Yb | 1.10 | 0.16 | | 2.54 | 3.81 | 3.79 | +1 |
| Lu | 0.21 | 0.03 | | 0.35 | 0.59 | 0.59 | |

| Sample 48 | Amp | Ep | Pl | Ttn | Total | Meas. | %Diff. |
|---|---|---|---|---|---|---|---|
| Mode % | 74 | 7 | 15 | 2 | | (+2%Quartz) | |
| | | Epidote amphibolite: reconstructed REE | | | | | |
| La ppm | 0.07 | 1.71 | 0.06 | 4.78 | 6.62 | 5.65 | +17 |
| Ce | 0.45 | 2.22 | 0.25 | 11.77 | 14.69 | 15.73 | –7 |
| Pr | 0.14 | 0.05 | 0.02 | 1.79 | 2.00 | 2.31 | –14 |
| Nd | 0.81 | 0.28 | 0.11 | 10.34 | 11.54 | 11.88 | –3 |
| Sm | 0.36 | 0.09 | 0.03 | 3.52 | 3.99 | 4.01 | –1 |
| Eu | 0.12 | 0.03 | 0.25 | 1.25 | 1.65 | 1.45 | +13 |
| Gd | 0.60 | 0.49 | 0.02 | 4.00 | 5.12 | 5.39 | –5 |
| Tb | 0.16 | 0.01 | 0.01 | 0.69 | 0.88 | 0.91 | –3 |
| Dy | 0.95 | 0.18 | 0.04 | 4.84 | 6.01 | 6.05 | –1 |
| Ho | 0.20 | 0.01 | 0.01 | 0.98 | 1.19 | 1.21 | –1 |
| Er | 0.81 | 0.05 | 0.03 | 2.68 | 3.57 | 3.58 | |
| Tm | 0.09 | 0.03 | | 0.40 | 0.52 | 0.52 | |
| Yb | 0.78 | 0.02 | 0.02 | 2.56 | 3.38 | 3.39 | –1 |
| Lu | 0.12 | 0.03 | | 0.39 | 0.54 | 0.54 | |

| Sample06 | Amp | Ep | Pl | Ttn | Total | Meas. | %Diff. |
|---|---|---|---|---|---|---|---|
| Mode % | 77 | 3 | 15 | 1 | | (+4% Quartz) | |
| | | Epidote amphibolite: reconstructed REE | | | | | |
| La ppm | 2.04 | 2.49 | 0.62 | 1.32 | 6.47 | 4.77 | +36 |
| Ce | 5.72 | 5.46 | 1.24 | 4.72 | 17.14 | 13.75 | +25 |
| Pr | 2.02 | 0.56 | 0.05 | 0.70 | 3.33 | 2.18 | +53 |
| Nd | 9.09 | 1.93 | 0.12 | 3.43 | 14.57 | 11.67 | +25 |
| Sm | 3.72 | 0.38 | 0.03 | 0.79 | 4.91 | 4.13 | +19 |
| Eu | 1.36 | 0.10 | 0.02 | 0.30 | 1.79 | 1.46 | +22 |
| Gd | 4.52 | 0.34 | 0.03 | 0.76 | 5.64 | 5.56 | |
| Tb | 0.77 | 0.04 | 0.01 | 0.08 | 0.89 | 0.98 | –9 |
| Dy | 5.54 | 0.23 | 0.05 | 0.34 | 6.15 | 6.65 | –7 |
| Ho | 1.12 | 0.04 | 0.01 | 0.04 | 1.21 | 1.35 | –10 |
| Er | 3.40 | 0.10 | 0.02 | 0.07 | 3.59 | 3.98 | –10 |
| Tm | 0.49 | 0.01 | | 0.12 | 0.62 | 0.57 | +10 |
| Yb | 3.18 | 0.04 | 0.01 | 0.57 | 3.80 | 3.75 | +1 |
| Lu | 0.62 | 0.01 | | 0.05 | 0.68 | 0.60 | +12 |

| Sample 49 | Amp | Pl | Ttn | Total | Meas. | %Diff. |
|---|---|---|---|---|---|---|
| Mode% | 65 | 29 | 1 | | (+5%Quartz) | |
| | | Plagioclase amphibolite: reconstructed REE | | | | |
| La ppm | 2.59 | 0.80 | 0.15 | 3.53 | 5.20 | –32 |
| Ce | 8.97 | 0.78 | 2.68 | 12.43 | 14.41 | –14 |
| Pr | 1.53 | 0.06 | 0.19 | 1.78 | 2.25 | –21 |
| Nd | 8.26 | 0.22 | 2.99 | 11.47 | 11.61 | –1 |
| Sm | 3.02 | 0.04 | 0.51 | 3.57 | 4.02 | –11 |
| Eu | 1.08 | 0.05 | 0.13 | 1.26 | 1.42 | –11 |
| Gd | 4.46 | 0.01 | 0.67 | 5.14 | 5.42 | –5 |
| Tb | 0.77 | | 0.11 | 0.88 | 0.92 | –5 |
| Dy | 5.47 | 0.01 | 0.76 | 6.25 | 6.00 | +4 |
| Ho | 1.19 | | 0.15 | 1.34 | 1.24 | +8 |
| Er | 3.58 | 0.02 | 0.46 | 4.06 | 3.68 | +10 |
| Tm | 0.51 | 0.01 | 0.07 | 0.58 | 0.54 | +8 |
| Yb | 3.59 | 0.01 | 0.51 | 4.11 | 3.63 | +13 |
| Lu | 0.52 | | 0.07 | 0.59 | 0.59 | |

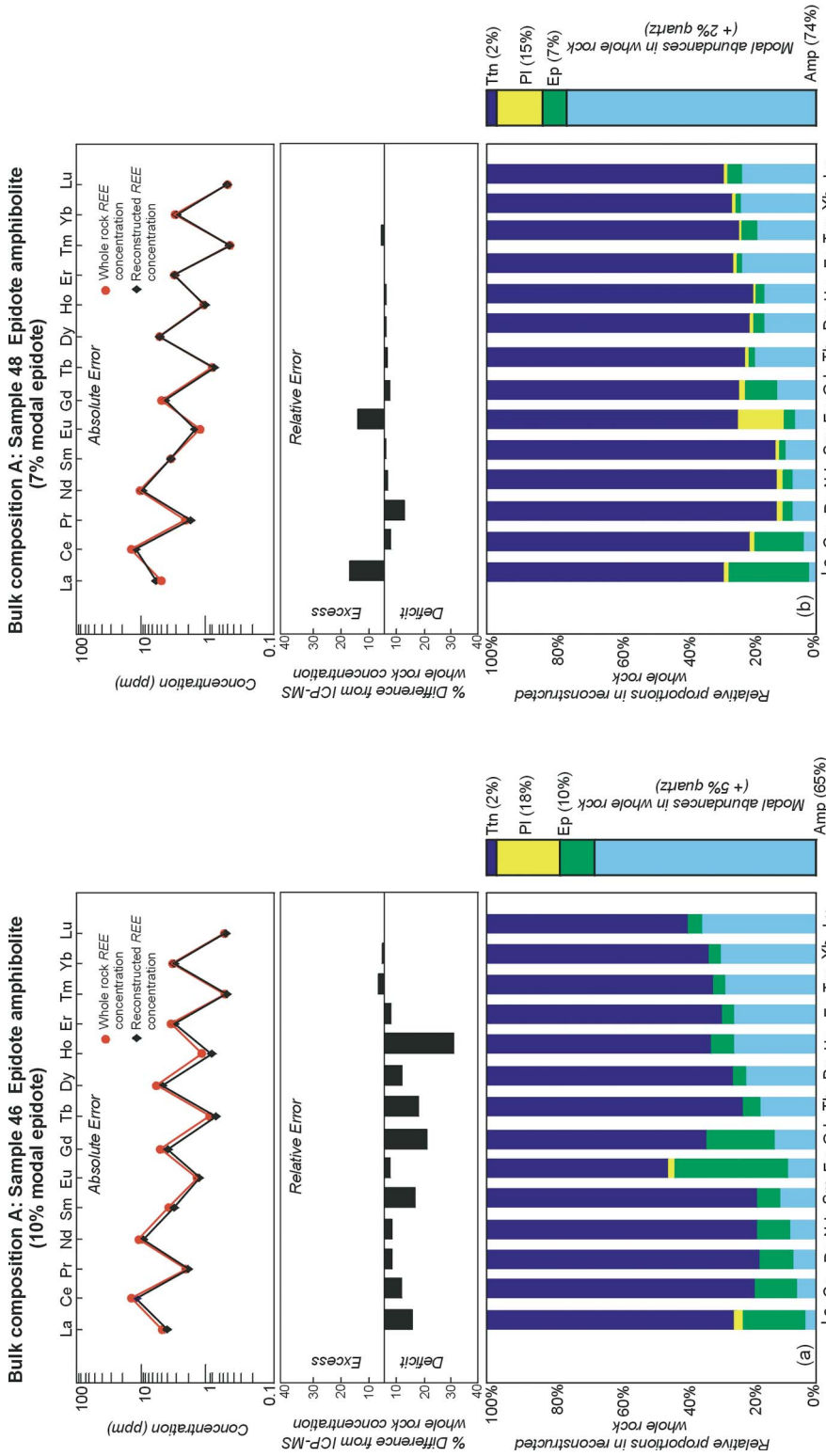


FIG. 12. (a–d) Mass-balance diagrams showing the relative roles of Ca amphibole, plagioclase, epidote, and titanite as carriers for the REE in four sample across the epidote-out isograd. Each figure comprises three parts. Top: illustration of the absolute errors between reconstructed and measured whole-rock concentrations. Middle: illustration of relative errors, given as % difference between reconstructed and measured REE concentrations. Bottom: stacked bar-graph illustrating the relative proportions of the REE in each phase.

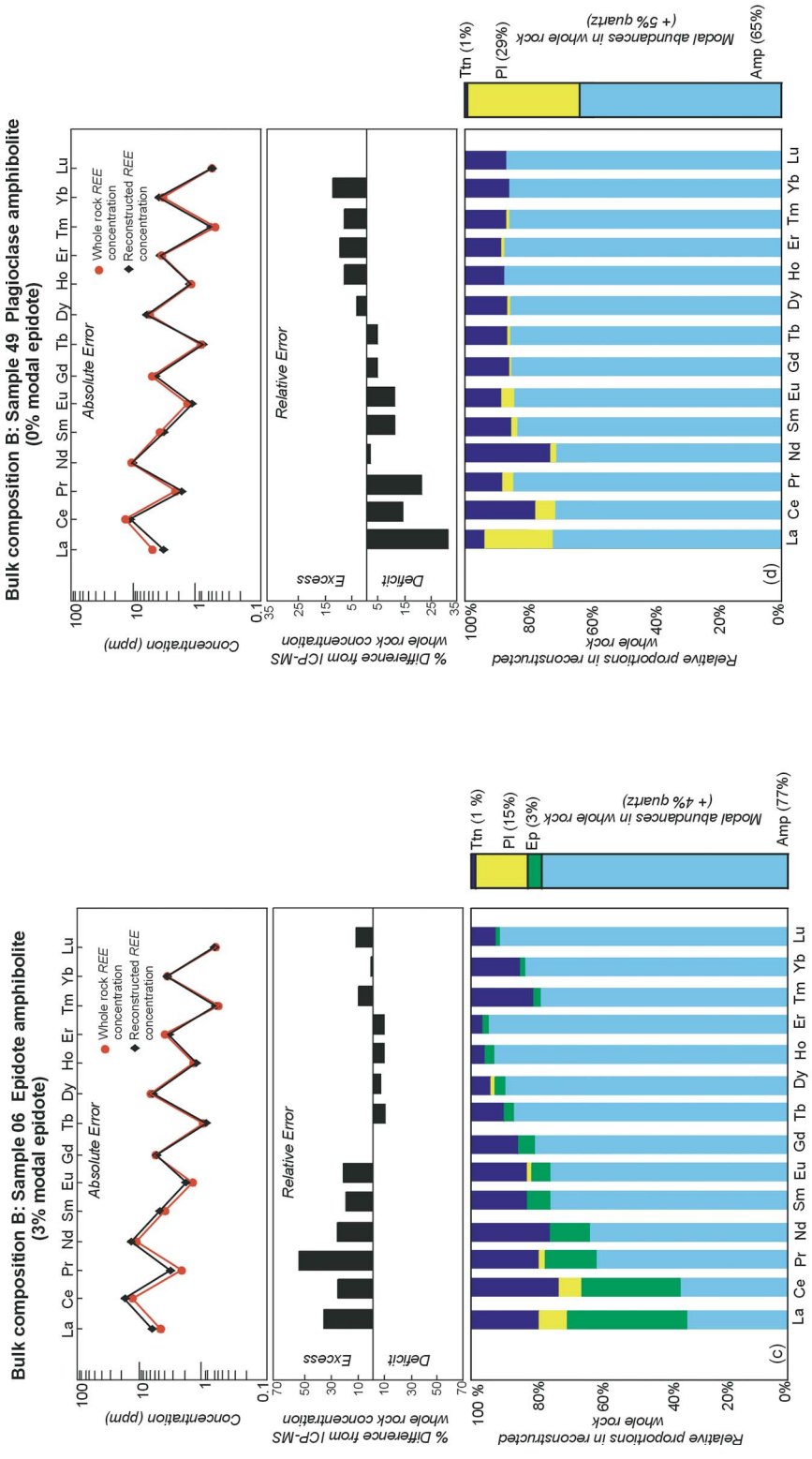
Bulk composition B: Sample 06 Epidote amphibolite
(3% modal epidote)
Bulk composition B: Sample 49 Plagioclase amphibolite
(0% modal epidote)
La Ce Pr Nd Sm Eu Gd Tb Dy Ho Er Tm Yb Lu
Absolute Error
Whole rock REE concentration
Reconstructed REE concentration
Concentration (ppm)
Relative Error
Excess
Deficit
% Difference from ICP-MS whole rock concentration
Relative proportions in reconstructed whole rock
(c)
(d)
Modal abundances in whole rock (+ 4% quartz)
Modal abundances in whole rock (+ 5% quartz)
Ttn (1 %)
Pl (15%)
Ep (3%)
Amp (77%)
Ttn (1%)
Pl (29%)
Amp (65%)

25% of the REE budget, favoring the LREE and two of the HREE (Tm and Yb). The role of plagioclase (15 modal %), although slightly increased compared to that in subgroup A, remains subordinate, accounting for <10% of LREE and Eu, and insignificant proportions of other elements. The REE budget in plagioclase amphibolite (sample 49) is distributed among only three phases (Ca amphibole, plagioclase, and titanite), but with respect to REE reservoirs, this sample exhibits similar behavior to sample 06, except that Ca amphibole has taken up the majority of the REE formerly held in epidote. Thus, Ca amphibole (65 modal %) is the dominant carrier for 70–85% of all the REE, slightly favoring the MREE and HREE. Plagioclase (29 modal %) carries 5–10% of the LREE, and titanite (1 modal %) accounts for 10–20% of the bulk-rock REE budget.

*Uncertainties*

Differences between measured and reconstructed whole-rock abundances of the REE could be due to inaccuracies in measured modal abundances, an unrepresentative choice of equilibrium compositions of minerals, within-sample variations in REE concentrations, or overlooked minor (<1% modal) REE carriers. We argue here that uncertainties in the estimated modal abundances of the minor phases titanite and epidote and within-sample variations in REE abundances of these phases (indicated by large standard deviations in Table 3) are the most likely causes. For instance, reconstructed budgets for some of the LREE in samples 48 (subgroup A) and 06 (subgroup B) exhibit small excesses (Figs. 12b–c). In these samples, most of the budgeted LREE reside in titanite and epidote, and minor overestimates in the modal abundance of epidote could explain the differences without producing large deficits in other elements. Similarly, considering the role of titanite in sequestering most of the REE in sample 46 (subgroup A, Fig. 12a) and 15–20% of the REE in sample 49 (subgroup B, Fig. 12d), the slight deficits in the reconstructed whole-rock budgets for most REE in these samples may be due to minor underestimations of the modal abundance of this phase or to the large standard deviations for some of its measured concentrations of the rare-earth elements.

*Mass-balance: discussion*

There are no significant mass gains or mass losses of the REE among analyzed samples (Table 1, Fig. 3b), and their systematic redistribution among coexisting phases (Table 5) is consistent with equilibrium partitioning of these elements during metamorphism. However, it is clear from the four samples that not only the assemblage and modal abundances of the coexisting phases, but also their bulk compositions (*i.e.*, subgroups A and B), and hence phase compositions, exhibit significant controls on REE partitioning. The most egregious example of the role of phase composition may be illustrated by comparing the relative carrier roles of "cummingtonite-rich" Ca amphibole from compositional subgroup A and "cummingtonite-poor" Ca amphibole from subgroup B. In subgroup A, titanite is the dominant carrier (50–80%) of all the REE, with "cummingtonite-rich" Ca amphibole taking approximately 30% of the HREE budget, epidote accounting for up to 20% of the LREE, and plagioclase having no significant role as a REE carrier. In contrast, in subgroup B, "cummingtonite-poor" Ca amphibole in both epidote amphibolite and plagioclase amphibolite is the dominant carrier (75 to 85%) of all the REE, with titanite accounting for most of the remaining MREE and HREE, and plagioclase (with epidote where present) carrying minor (<15%) amounts of the LREE. When considered in the context of the modal abundances of Ca amphibole in the four samples, which do not show any consistent trend, these results demonstrate the important role of amphibole composition in determining REE uptake.

A second example of compositional control on REE uptake is exhibited by plagioclase. Where richer in An (subgroup B), the plagioclase carries more LREE than An-poorer plagioclase (subgroup A), which in this case is attributed both to its higher modal abundance, and to the compositional control imposed by the An component on the structure, which induces a structural distortion of the *A* site, rendering it closer in size to the ionic radius of the LREE. The decrease in the REE concentration of plagioclase in plagioclase amphibolite (sample 49) relative to epidote amphibolite (sample 06; Table 3) is interpreted as a dilution effect due to the approximate doubling of modal plagioclase between the two samples.

Similarly, REE contents in epidote are correlated with $X_{Czo}^{Ep}$, being greater in subgroup B than A, but no correlation between REE content and titanite composition was found. Figure 13 provides a visual assessment of the changing average carrier roles of the four phases between subgroups A and B. In addition, changes in the behavior of each phase with respect to the presence or absence of epidote can be assessed. The major increase in the role of Ca amphibole as a carrier for all the REE, the significant increase in the role of plagioclase as a carrier for the first two LREE (La and Ce), and the concomitant decrease in the role of titanite as a carrier for all the REE, are readily observed in these figures. In addition, the increased role of epidote as a LREE carrier in bulk composition B (sample 06), despite its reduced modal abundance, is apparent.

Thus, the distribution of the REE among these samples is linked to a subtle interplay among whole-rock composition, major-element composition of minerals, the assemblage of minerals and their modal abundance.

*Reaction balancing: matrix analysis of the epidote-out reaction isograd*

The petrological applications of matrix analysis by singular value decomposition (SVD) were introduced by Fisher (1989) and have since been used to quantitatively model changes in metamorphic assemblages at reaction isograds (*e.g.*, Gordon *et al.* 1991, Hartel & Pattison 1996, Cesare 1999). SVD analysis is employed on pairs of mineral assemblages to search for a single, hypothetical bulk-composition that can be expressed as a combination of the mineral compositions in each assemblage. In principle, this is equivalent to the search for a mass balance between the two assemblages. With respect to this study, if such a balanced "reaction" exists between assemblages of subgroups A and B, it is permissive, albeit not diagnostic, that the epidote-out isograd is due to a change in externally imposed conditions, *i.e.*, *T*, or *P*, or both (Greenwood 1967, 1968, Gordon *et al.* 1991). If such a balanced reaction is present, it can then be used to model the redistribution of the REE formerly sequestered in epidote in epidote amphibolite to coexisting phases in plagioclase amphibolite above the reaction isograd.

*Initial subjective assumptions and methods*

In the qualitative epidote-out reaction, R1, it was inferred that the major elements sequestered in epidote were largely taken up by slight adjustments to the compositions and modal abundances of Ca amphibole and plagioclase, with the role of titanite being unclear. Quartz is indicated on both sides of the reaction as it is not known whether it was a reactant or product in this $SiO_2$-saturated system. The presence of OH-bearing phases on both sides of the reaction, together with the inference of $H_2O$ as a product of the reaction and the absence of carbonates in all the assemblages, can be interpreted to suggest that to a first approximation, the system was $H_2O$-saturated.

SVD matrix analysis using the mineral assemblages in samples 46 (A) and 49 (B) was performed with version 4 of Mathematica®. Input data were the average major-element compositions of Ca amphibole, epidote, plagioclase and titanite in these samples, as determined by EPMA, and expressed as numbers of atoms per formula unit (Table 2). The seven phases in the model reaction account for approximately 95% of the modes of samples 46 and 49, with the remaining 5% occurring

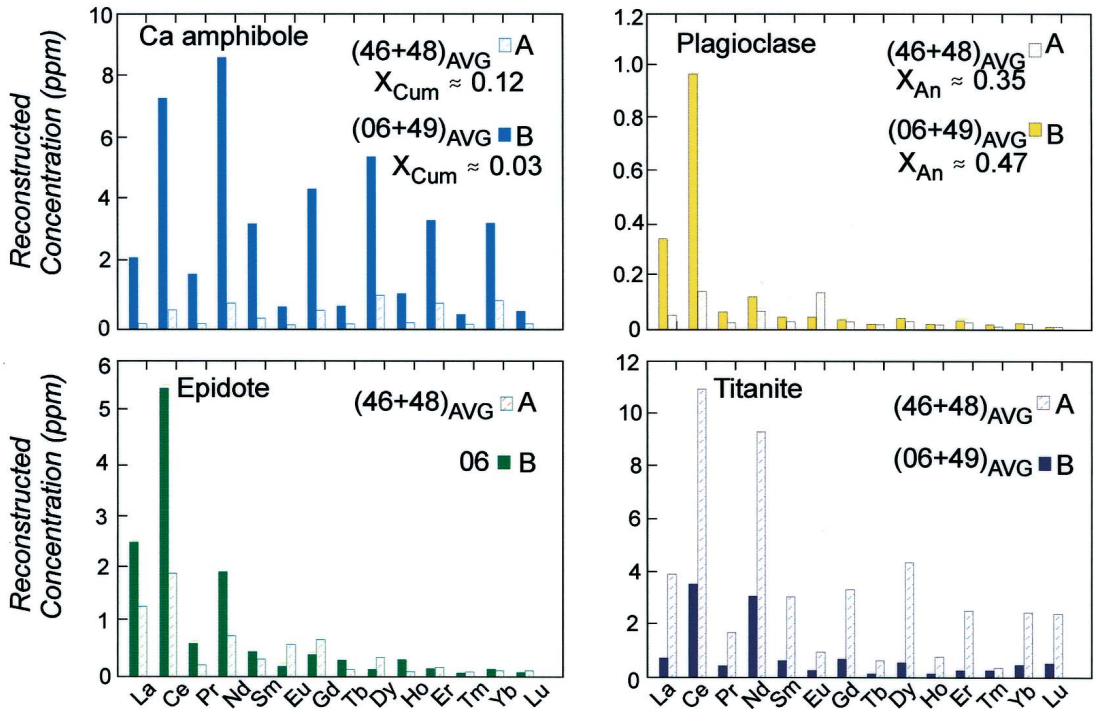


FIG. 13. Average reconstructed concentrations of the REE (measured average concentration times the modal abundance) in Ca amphibole, plagioclase, epidote and titanite for samples in compositional subgroups A and B.

mainly as quartz. The presence of minor (<1%) sulfide, ilmenite, or zircon is possible, but these minerals, and the system components required to produce them, are ignored in this analysis as they are not considered to be significant participants in the overall isograd reaction.

The compositional variability of these seven phases in the composite matrix is described in terms of the nine cations ($Ti^{4+}$, $Al^{3+}$, $Fe^{3+}$, $Fe^{2+}$, $Mg^{2+}$, $Mn^{2+}$, $Ca^{2+}$, $Na^{+}$, $K^{+}$), that have been combined to yield six independent components ($Ti^{4+}$, $Al^{3+}$, $Fe^{3+}$, $\Sigma(Fe,Mg,Mn)^{2+}$, $Ca^{2+}$, and $\Sigma(Na,K^{+})$. Silicon was omitted from the compositional matrix because quartz is in excess in this system, and a similar argument can be extended to the omission of $H^{+}$ due to the inferred presence of intergranular $H_2O$ (Fisher 1989). Ferrous iron, $Mg^{2+}$ and $Mn^{2+}$ are summed, as they occur in significant abundance only in Ca amphibole, *i.e.*, they are not partitioned between two or more phases. Potassium, a very minor component of this system, has been summed with $Na^{+}$, as these two elements substitute for each other in Ca amphibole and plagioclase. The proportion of ferric iron was calculated on a stoichiometric basis using the procedure of Spear (1993). Aluminum and $Fe^{3+}$ are treated as independent components because they are partitioned among Ca amphibole, plagioclase, and epidote in different proportions.

Since interpretation of the results is based on whether or not a mass balance can be found within compositional uncertainty, the slightly larger uncertainties resulting from averaging mineral compositions over the entire thin-section scale make it more likely to obtain a mass balance. On the other hand, the scale of inferred equilibrium is larger than if results of single-spot analyses from smaller areas of the thin section were utilized, possibly rendering the results more generally applicable.

Following Hartel & Pattison (1996), the absolute deviations from perfect balance of cations for each constituent are compared with the analytical uncertainty and the reaction is considered adequately balanced if the result is within 3σ analytical errors. The compositional matrix used in the SVD determination was unweighted to prevent undue influence of minor constituents (Gordon *et al.* 1991).

## Phase-Rule Variance of Assemblages

The assumption that minerals in abundant and widespread assemblages attained equilibrium under divariant conditions can be tested by a determination of the variance of the assemblage. The number of components ($c$) in a thermodynamic system is equal to the rank of the matrix of vectors that expresses the compositions of phases in terms of an initial set of constituents (Gordon *et al.* 1991), which in this study are the number of cations per formula unit in each mineral in the two assemblages. Fisher (1989) showed that a variance of less than two means that one or more mass balances can be written for some or all of the phase combinations of the assemblage. As a result of our initial choice of independent components for the epidote amphibolite (#46) and plagioclase amphibolite (#49) assemblages studied here, there is a 6 row × 7 column matrix formed by columns of the compositions of each phase. In order to yield a univariant reaction, or mass balance, the SVD of the compositional matrix is required to have a rank of 6 (*i.e.*, $c = 6$).

### *Results*

The 6 × 7 composite compositional matrix (**M**), the resultant stoichiometric reaction-coefficients, the reconstructed cation totals derived by multiplying the elements of the composition matrix by the appropriate stoichiometric coefficients, and the error estimates, given as the percent deviation from perfect mass-balance between reactant and product assemblages, are summarized in Tables 6.1–6.4. SVD analysis of **M** yields six nonzero singular values, indicating a rank of 6. According to the phase rule, the variance of the system is therefore 1, so it is not necessary to calculate a model matrix ($\mathbf{M}^{\prime}$) of reduced rank to represent the original composition matrix (Fisher 1989). In this situation, a mass balance between samples 46 and 49 is implied. Normalizing the reaction coefficients to one for $Ep_{46}$, the reaction is:

$$2.94\ CaAmp_{46} + 5.0\ Pl_{46} + 1\ Ep_{46} + 5.21\ Ttn_{46} = 3.14\ CaAmp_{49} + 5.65\ Pl_{49} + 5.29\ Ttn_{49} \qquad (R2)$$

Since the calculation of a model matrix of reduced rank was not necessary to satisfy the condition of univariant equilibrium, there are no residuals to compare to 1σ analytical uncertainties. However, by multiplying the columns of the composite compositional matrix by the appropriate stoichiometric coefficients from R2, the reconstructed cation totals are obtained (Table 6) which, when summed for all the phases in samples 46 and 49, represent the numbers of each species of cation on either side of the mass-balanced reaction. The percentage difference between these numbers for each cation species is used to estimate the quality of the reaction balance. In all cases, the errors are within three times the 1σ analytical uncertainty of the EPMA analyses (Table 6.3–6.4). The percent absolute deviation of the total number of cations with respect to an arbitrary side of the model reaction (here "reactant" side, *i.e.*, #46) is within 1% relative difference. If viewed in this manner, the model reaction R2 can be interpreted as conveying something close to univariant equilibrium.

Following the reasoning of Gordon *et al.* (1991), the implied univariant equilibrium relationship between these epidote amphibolite and plagioclase amphibolite assemblages is permissive that the epidote-out isograd is due to a change in externally imposed conditions, *i.e.*, $T$, or $P$, or both, and not to bulk-composition differences between subgroups A (#46) and B (#49). From a geo-

logical perspective, R2 also is a reasonable representation of the textures and modal variations observed in natural samples throughout the field area (Jamieson 1979, Mulrooney 2004), *i.e.*, it is a reaction isograd following the definition of Carmichael (1969). For example, the breakdown of epidote is linked to increases in the reaction coefficients for Ca amphibole and plagioclase, compatible with the previous inference that major elements sequestered in epidote (*e.g.*, Ca, Al, $Fe^{3+}$) contribute to increased modal abundances of these phases above the isograd. On the other hand, R2 indicates a slight increase in modal titanite on the product side, which is not supported by measurements of modal abundance. The measured reduction in the modal abun-

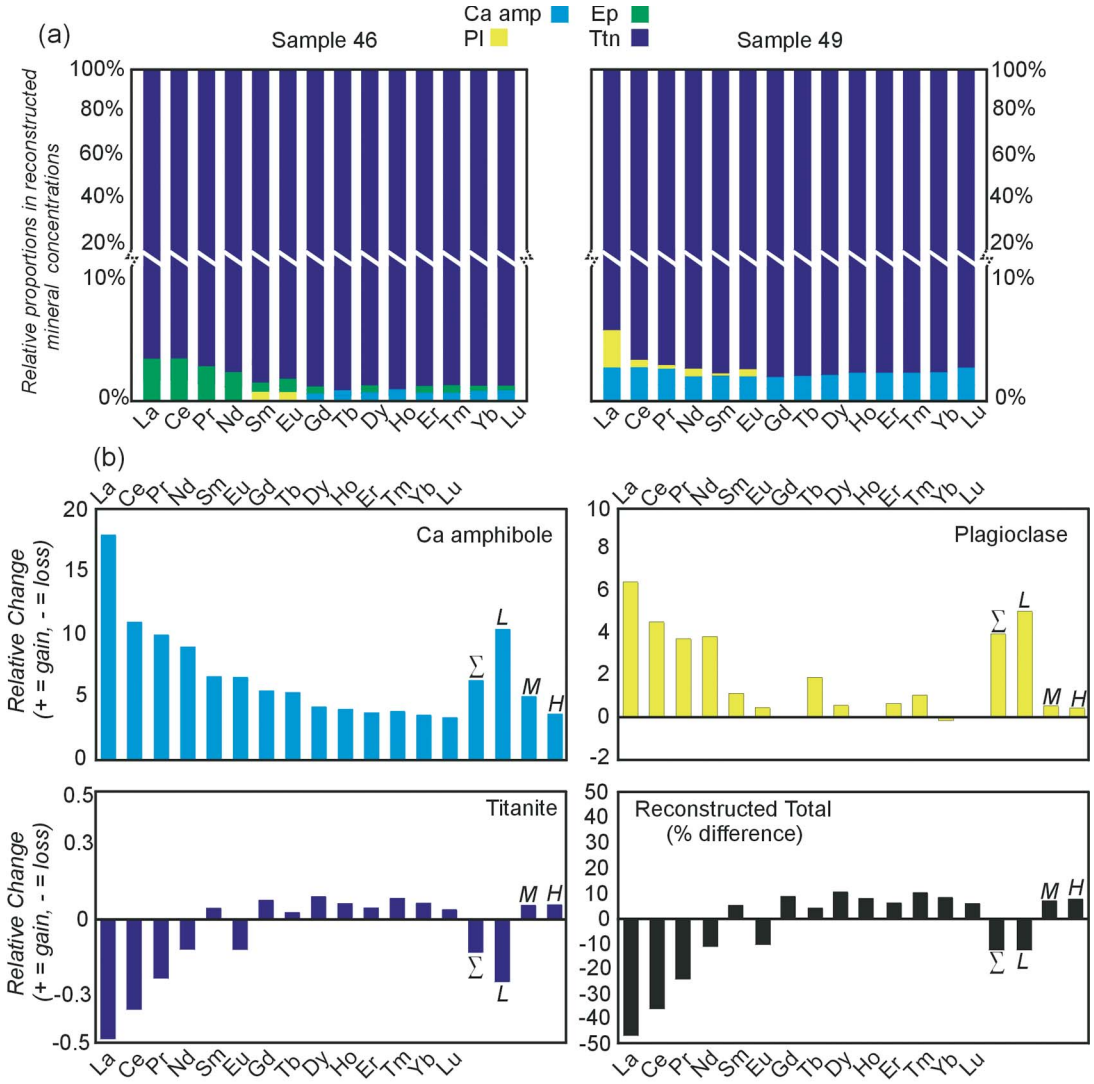


FIG. 14. (a) Bar graphs illustrating the relative proportions of the REE in each phase in sample 46 (below the epidote-out isograd) and sample 49 (above the isograd) on the basis of the model epidote-out reaction. (b) Bar graphs illustrating the relative differences in reconstructed REE abundances in minerals (measured abundance times the stoichiometric coefficient) in Ca amphibole, plagioclase and titanite above the isograd (sample 49), compared to reactant assemblage (sample 46), and the percent difference of the sums of the reconstructed totals of the REE in all phases (including epidote) in the product assemblage compared to the reactant assemblage. L, M, and H denote LREE, MREE, and HREE respectively; Σ denotes ΣREE.

dance of titanite in plagioclase amphibolite is due to an independent reaction, unrelated to the breakdown of epidote.

TABLE 6. MODEL MASS-BALANCED REACTION ACROSS THE EPIDOTE-OUT "REACTION" ISOGRAD (TOP) BASED ON SVD ANALYSIS OF COMPOSITE COMPOSITIONAL MATRIX (M) [TABLE 6.1] DERIVED FROM AVERAGE COMPOSITIONS OF MINERALS IN SAMPLES 46 (EPIDOTE AMPHIBOLITE) AND 49 (PLAGIOCLASE AMPHIBOLITE). RECONSTRUCTED CATION TOTALS [TABLE 6.2] BASED ON MEASURED MINERAL ABUNDANCES (TABLE 4.1) AND CALCULATED REACTION-COEFFICIENTS. RECONSTRUCTED ΣCATIONS [TABLE 6.3] OBTAINED BY SUMMING THESE VALUES FOR EACH SIDE OF THE REACTION. DIFFERENCES IN RECONSTRUCTED TOTALS BETWEEN REACTANT AND PRODUCT SIDES OF THE REACTION ARE GIVEN AS % DIFFERENCE AND ABSOLUTE DIFF [TABLE 6.3], WHICH ARE COMPARED AT THE 1σ AND 3σ LEVELS WITH THE ANALYTICAL ERROR ASSOCIATED WITH EPMA ANALYSIS [TABLE 6.4]

$$2.94\ Ca\ amp_{46} + 5.00\ Pl_{46} + 1.00\ Ep_{46} + 5.21\ Ttn_{46} = 3.14\ Ca\ amp_{49} + 5.65\ Pl_{49} + 5.29\ Ttn_{49}$$

Table 6.1. Composite Compositional Matrix (M)

| | $Ca\ amp_{46}$ | $Pl_{46}$ | $Ep_{46}$ | $Ttn_{46}$ | $Ca\ amp_{49}$ | $Pl_{49}$ | $Ttn_{49}$ |
|---|---|---|---|---|---|---|---|
| Ti | 0.11 | 0.00 | 0.00 | 0.94 | 0.12 | 0.00 | 0.93 |
| Al | 2.11 | 1.31 | 2.30 | 0.05 | 2.26 | 1.40 | 0.07 |
| $Fe^{3+}$ | 0.02 | 0.00 | 0.81 | 0.00 | 0.29 | 0.00 | 0.01 |
| FeMgMn | 4.48 | 0.02 | 0.01 | 0.01 | 4.18 | 0.03 | 0.00 |
| Ca | 1.76 | 0.34 | 2.03 | 1.01 | 1.94 | 0.48 | 0.99 |
| NaK | 0.61 | 0.68 | 0.00 | 0.00 | 0.79 | 0.47 | 0.00 |

Table 6.2. Reconstructed Cation Totals

| | $Ca\ amp_{46}$ | $Pl_{46}$ | $Ep_{46}$ | $Ttn_{46}$ | $Ca\ amp_{49}$ | $Pl_{49}$ | $Ttn_{49}$ |
|---|---|---|---|---|---|---|---|
| Ti | 0.11 | 0.00 | 0.00 | 1.66 | 0.13 | 0.00 | 1.67 |
| Al | 2.11 | 2.23 | 0.78 | 0.09 | 2.42 | 2.69 | 0.13 |
| $Fe^{3+}$ | 0.02 | 0.00 | 0.28 | 0.00 | 0.31 | 0.00 | 0.02 |
| FeMgMn | 4.48 | 0.03 | 0.00 | 0.02 | 4.47 | 0.06 | 0.00 |
| Ca | 1.76 | 0.58 | 0.69 | 1.79 | 2.08 | 0.92 | 1.78 |
| NaK | 0.61 | 1.16 | 0.00 | 0.00 | 0.85 | 0.90 | 0.00 |

Table 6.3. Reconstructed ΣCations

| | 46 | 49 | Diff (%) | Diff* | *Diff @ 1 σ* | *Diff @ 3 σ* |
|---|---|---|---|---|---|---|
| Ti | 1.77 | 1.80 | 1.61 | 0.03 | 0.05 | 0.15 |
| Al | 5.21 | 5.23 | 0.47 | 0.02 | 0.01 | 0.03 |
| $Fe^{3+}$ | 0.30 | 0.33 | 11.14 | 0.03 | 0.01 | 0.03 |
| FeMgMn | 4.54 | 4.53 | 0.11 | 0.005 | 0.02 | 0.06 |
| Ca | 4.76 | 4.78 | 0.30 | 0.01 | 0.06 | 0.18 |
| NaK | 1.77 | 1.75 | 1.04 | 0.02 | 0.07 | 0.21 |
| Total | 18.34 | 18.42 | 0.68 | 0.12 | 0.06 | 0.18 |

Table 6.4. 1 σ errors (EPMA)

| | $Ca\ amp_{46}$ | $Pl_{46}$ | $Ep_{46}$ | $Ttn_{46}$ | $Ca\ amp_{49}$ | $Pl_{49}$ | $Ttn_{49}$ |
|---|---|---|---|---|---|---|---|
| Ti | 0.01 | 0.001 | 0.003 | 0.01 | 0.004 | 0.001 | 0.04 |
| Al | 0.03 | 0.03 | 0.03 | 0.01 | 0.04 | 0.03 | 0.04 |
| $Fe^{3+}$ | 0.04 | 0.001 | 0.04 | 0.004 | 0.05 | 0.001 | 0.001 |
| FeMgMn | 0.03 | 0.02 | 0.001 | 0.001 | 0.07 | 0.01 | 0.01 |
| Ca | 0.03 | 0.03 | 0.03 | 0.01 | 0.03 | 0.03 | 0.05 |
| NaK | 0.04 | 0.03 | 0.01 | 0.01 | 0.03 | 0.04 | 0.001 |

* Absolute values of differences between samples 49 ("products") and 46 ("reactants"). See text and Figure 14 for additional explanations.

Despite the fact that R2 provides a reasonable model for observed variations in modal and major-element mineral compositions in these rocks, there is no guarantee that this specific reaction occurred. In fact, a similar result has been achieved using sample 48 instead of 46, suggesting that R2 may represent the "sum" of a multi-stage reaction-history, perhaps involving an approximately discontinuous epidote-consuming reaction, followed by subtle exchange-reactions among Ca amphibole, plagioclase, and possibly titanite. Nevertheless,

TABLE 7. REDISTRIBUTION OF RARE-EARTH ELEMENTS AMONG ANALYZED PHASES USING THE BALANCED MODEL EPIDOTE-OUT REACTION

| REE Reconstructed | $Ca\ amp_{46}$ | $Pl_{46}$ | $Ep_{46}$ | $Ttn_{46}$ | $Ca\ amp_{49}$ | $Pl_{49}$ | $Ttn_{49}$ |
|---|---|---|---|---|---|---|---|
| La ppm | 0.22 | 0.48 | 12.18 | 236.2 | 4.08 | 3.50 | 124.1 |
| Ce | 1.18 | 0.65 | 23.59 | 749.3 | 13.91 | 3.56 | 482.8 |
| Pr | 0.22 | 0.06 | 3.06 | 113.1 | 2.42 | 0.30 | 86.7 |
| Nd | 1.44 | 0.20 | 12.38 | 605.3 | 13.99 | 0.95 | 538.2 |
| Sm | 0.66 | 0.06 | 2.30 | 199.9 | 4.95 | 0.13 | 208.0 |
| Eu | 0.23 | 0.15 | 0.81 | 70.27 | 1.65 | 0.22 | 62.55 |
| Gd | 1.12 | 0.07 | 1.72 | 269.0 | 7.00 | 0.06 | 288.5 |
| Tb | 0.19 | 0.00 | 0.23 | 46.20 | 1.18 | 0.01 | 47.25 |
| Dy | 1.66 | 0.03 | 1.41 | 324.5 | 8.29 | 0.05 | 352.8 |
| Ho | 0.37 | 0.00 | 0.26 | 66.20 | 1.77 | 0.01 | 70.11 |
| Er | 1.15 | 0.03 | 0.69 | 195.7 | 5.16 | 0.05 | 204.3 |
| Tm | 0.17 | 0.01 | 0.09 | 27.49 | 0.76 | 0.01 | 29.71 |
| Yb | 1.24 | 0.05 | 0.60 | 188.2 | 5.30 | 0.05 | 199.9 |
| Lu | 0.21 | 0.00 | 0.09 | 25.67 | 0.84 | 0.01 | 26.60 |
| LREE | 3.06 | 1.39 | 51.20 | 1703 | 34.40 | 8.32 | 1231.7 |
| MREE | 4.22 | 0.33 | 6.73 | 976.1 | 24.84 | 0.48 | 1029.2 |
| HREE | 2.75 | 0.09 | 1.46 | 437.0 | 12.06 | 0.13 | 460.6 |
| ΣREE | 10.03 | 1.81 | 59.40 | 3116 | 71.30 | 8.93 | 2722 |

| REE | Relative Enrichment-Factor (#49 – #46) / #46 | | | Reconstructed Total (ppm) | | Diff. (%) {(Σ49–Σ46)/ Σ46}*100 |
|---|---|---|---|---|---|---|
| | Ca amp | Pl | Ttn | 46 | 49 | |
| La | 17.92 | 6.37 | -0.47 | 249.1 | 131.7 | -47.14 |
| Ce | 10.80 | 4.49 | -0.36 | 774.7 | 500.2 | -35.43 |
| Pr | 9.81 | 3.70 | -0.23 | 116.5 | 89.40 | -23.23 |
| Nd | 8.73 | 3.80 | -0.11 | 619.4 | 553.1 | -10.69 |
| Sm | 6.50 | 1.10 | 0.04 | 202.9 | 213.1 | 5.00 |
| Eu | 6.25 | 0.42 | -0.11 | 71.46 | 64.42 | -9.85 |
| Gd | 5.27 | -0.20 | 0.07 | 271.9 | 295.5 | 8.66 |
| Tb | 5.16 | 1.86 | 0.02 | 46.62 | 48.44 | 3.89 |
| Dy | 3.99 | 0.51 | 0.09 | 327.6 | 361.1 | 10.24 |
| Ho | 3.82 | | 0.06 | 66.82 | 71.89 | 7.58 |
| Er | 3.49 | 0.65 | 0.04 | 197.6 | 209.5 | 6.04 |
| Tm | 3.59 | 1.02 | 0.08 | 27.75 | 30.48 | 9.83 |
| Yb | 3.29 | -0.04 | 0.06 | 190.0 | 205.3 | 8.05 |
| Lu | 3.08 | | 0.04 | 25.96 | 27.45 | 5.76 |
| LREE | 10.26 | 5.00 | -0.28 | 1760 | 1274 | -27.57 |
| MREE | 4.88 | 0.47 | 0.05 | 987.4 | 1054 | 6.79 |
| HREE | 3.38 | 0.38 | 0.05 | 441.3 | 472.8 | 7.13 |
| ΣREE | 6.11 | 3.94 | -0.13 | 3189 | 2801 | -12.13 |

Reconstructed concentrations based on measured abundances (Table 3) and calculated reaction-coefficients (Table 6). Percent deviation from perfect mass-balance and relative enrichment factors for Ca amphibole, plagioclase and titanite based on the relative differences of reconstructed REEs between product and reactant sides of reaction 2. See text for explanations.

R2 is a plausible first-order model of the overall epidote-out reaction and provides a basis for the evaluation of the redistribution of the REE across the reaction isograd.

*Redistribution of the REE across the model epidote-out reaction isograd*

The stoichiometric coefficients of R2 can be multiplied by measured concentrations of the REE in minerals to model their redistributions across the epidote-out isograd, thereby enabling an estimate of the *relative changes* in REE abundances in minerals on either side of the reaction isograd (arbitrarily calculated with respect to the "reactant" side, *i.e.*, sample 46; Table 7). As with the major cations, the *percent absolute deviation* of the ΣREE is used to evaluate the overall "balance" of the reconstructed concentrations. Figure 14 provides a convenient way of illustrating the redistribution of the REE formerly sequestered in epidote to Ca amphibole, plagioclase, and titanite above the isograd. From the stacked bar-graphs (Fig. 14a), which illustrate the relative proportions of REE in each phase on both sides of the reaction isograd, it is clear that titanite overwhelmingly accounts for the majority of the REE in both reactants and products, *i.e.*, approximately 95% of LREE and 98% of the MREE and HREE budgets in sample 46, although its role is slightly diminished in sample 49 above the isograd. However, the most important changes in REE carrier roles occur among the other phases, *i.e.*, below the isograd, epidote and Ca amphibole account for almost all the remaining LREE and MREE and HREE, respectively, whereas above the isograd, the roles of Ca amphibole as a carrier for all the REE and plagioclase as a carrier for La and Eu increase significantly. We infer that on crossing the isograd, the breakdown of epidote changed the effective bulk-compostion available to these phases by infusing it with additional REE, especially the LREE. Thus on a molar basis, the changes in REE patterns in Ca amphibole and plagioclase resulting from the breakdown of epidote can be largely accounted for by the net transfer of the REE from epidote to these phases.

This first-order conclusion is further investigated in Figure 14b, in which it is clear that epidote breakdown cannot be separated from a significant reduction of LREE abundance in titanite, the most REE-enriched phase, so that the redistributed REE across the isograd do not come uniquely from epidote. Ca amphibole (~10 times) and plagioclase (~5 times) both exhibit significant increases in LREE abundance above the isograd (Table 3), which can thus be attributed to both the breakdown of epidote and the approximately 30% reduction in LREE abundance in titanite. As noted previously, the increased LREE-carrying capacities of Ca amphibole and plagioclase are linked to crystal-chemical changes in these phases as the isograd is crossed, *i.e.*, increasing Ca contents of the REE-hosting *M*4 site (Ca amphibole) and *A* site (plagioclase) respectively, rendering their sizes more appropriate for LREE substitution. This increased propensity of Ca amphibole and plagioclase to sequester the LREE thus correlates with changes in chondrite-normalized LREE abundances in titanite and in the slope of the $D^*_{REE}{}^{Amp/Ttn}$ partitioning across the epidote-out isograd (Figs. 7d and 8a, respectively), and is presumably also the cause of the slight decrease in LREE abundance in titanite above the isograd.

Table 7 and Figure 14 show that overall there is an approximate 12% deficit in reconstructed ΣREE abundances on a molar basis above the isograd. Most of this error is attributed to the relatively large deficit (~28%) in the reconstructed abundance of the LREE, as the errors for the MREE and HREE are relatively small (both ~7% in excess). In theory, the deficit in the LREE above the isograd could indicate that part of the LREE was lost during progressive metamorphism, but such an inference is not compatible with the measured LREE bulk-rock concentrations, which are essentially identical between the two samples (Table 1, Fig. 3b). Thus, the deficit may indicate that the measured average LREE concentrations are not perfectly representative, as with the mineral compositions chosen for the mass balance, or that some LREE formerly sequestered in epidote entered additional unrecognized LREE-bearing minor phase(s) above the isograd.

In summary, the model epidote-out reaction R2 accounts well for the redistribution of MREE and HREE across the reaction isograd. Titanite is the most REE-enriched phase on both sides of the isograd, but its MREE:LREE ratio rises as the isograd is crossed, which we relate to the increased affinity of LREE for Ca amphibole and plagioclase as a result of changes in the sizes of their *M*4- and *A*-site cavities, respectively. The Ca amphibole exhibits a significant increase in ΣREE (~six times), especially the LREE (~ten times) above the isograd as does plagioclase (~six times LREE), which are thus linked to both the increased availability of LREE following epidote breakdown and to crystal-chemical changes in these phases with increasing metamorphic grade.

## Conclusions

The principal conclusions resulting from this study are as follows:

1. Calcic amphibole, plagioclase, epidote and titanite exhibit a close approach to equilibrium partitioning of REE, as indicated by the general consistency in partitioning ratios within and between samples.

2. The REE contents in analyzed Ca amphibole, epidote and plagioclase exhibit systematic correlations with major-element compositions. In some cases, variations in major-element composition affect REE substitution at the same site: for example, the ratio of LREE to HREE in both plagioclase and Ca amphibole exhibits dependence on the Ca content of the plagioclase at the

*A* site and the extent of cummingtonite substitution affecting the *M*4 site of the Ca amphibole. In other cases, major-element variations at one site can affect REE incorporation at adjacent sites in the same mineral: for example, the ΣLREE at *X* sites in epidote is correlated with $^{VI}$Al at adjacent *M*3 sites. These relationships imply that simple formulations of geothermometers based solely on partitioning of REE between any two coexisting phases are unlikely to be forthcoming.

3. Site characteristics (ideal radius and elasticity) can be qualitatively approximated from $D^*_{REE}{}^{Min1/Min2}$ in Onuma-type diagrams, but quantitative estimates of these parameters cannot be extracted using the equation of Blundy & Wood (1994) for the minerals studied. On the basis of data in this study, we show that the REE in plagioclase, epidote and titanite are accommodated at single elastic sites with approximate ideal $r_0$ values of 1.18, 1.16 and 1.07 Å, respectively, whereas in Ca amphibole, they are accommodated at two sites, the *M4* site, with an $r_0$ of ~1.12 Å, and the *M*4' site, with an $r_0$ of ~1.03 Å, yielding the two measured types of REE patterns in Ca amphibole as a function of $X_{Cum}{}^{Amp}$.

4. Within analytical error, there is no measurable change in whole-rock ΣREE and LREE/HREE values across the epidote-out isograd, which implies that metamorphism was essentially isochemical with respect to the REE. In favorable cases, therefore, the REE act as relatively "immobile" elements, despite major redistribution among the coexisting metamorphic phases.

5. Results of a mass-balance study show that REE carriers are sensitive to small variations in bulk composition, with titanite and epidote being the main carriers of the REE in a relatively calcium-enriched bulk-composition, whereas Ca amphibole is the major carrier of the REE, with plagioclase assuming a minor role for the LREE in a slightly less calcium-rich bulk-composition The disappearance of epidote at the epidote-out isograd, in combination with modal and chemical changes in Ca amphibole and plagioclase, directly affects the REE-carrying capacities of these phases. These results suggest that incremental changes in *P*, *T*, *X*, and *M* all have significant implications for the redistribution of trace elements at and near metamorphic isograds.

6. Mass-balance analysis on a composite compositional matrix yielded the following model univariant reaction between epidote amphibolite (sample 46) and plagioclase amphibolite (sample 49) assemblages (assuming that $SiO_2$ is in excess, and $H_2O$ is a product phase): 2.94 $CaAmp_{46}$ + 5.0 $Pl_{46}$ + 1.00 $Ep_{46}$ + 5.21 $Ttn_{46}$ = 3.14 $CaAmp_{49}$ + 5.65 $Pl_{49}$ + 5.29 $Ttn_{49}$. The reaction suggests that the presence or absence of epidote is dominantly controlled by externally imposed conditions (*i.e.*, *P*, or *T*, or both) and not by slight variations in bulk chemical composition between the two samples, *i.e.*, the epidote-out reaction is a *reaction isograd*.

7. The breakdown of epidote across the epidote-out reaction isograd changed the effective bulk-composition of the model system by infusing it with REE, especially the LREE. Changes in REE patterns in Ca amphibole and plagioclase resulting from the breakdown of epidote can largely be accounted for by the net transfer of the REE from epidote to those phases, coupled with major-element crystal-chemical changes, *i.e.*, the presence of increased Ca at the *M*4 and *A* sites in Ca amphibole and plagioclase, respectively, which rendered these sites more suitable to host the REE. However, a significant reduction in LREE abundance in titanite above the isograd implies that the redistributed REE did not come uniquely from epidote. The increased propensity of Ca amphibole and plagioclase to sequester the LREE is inferred to be the cause of the corresponding decrease in LREE abundance in titanite above the isograd.

## Acknowledgements

It is a pleasure to submit this contribution to the special volume honoring Dugald Carmichael, whose innovative thinking and enthusiasm have inspired a generation of metamorphic petrologists. This study forms part of the M.Sc. thesis of the first author. We acknowledge the contributions of Pam King, Lakmali Hewa, Maggy Piranian, Mike Tubrett and Glen Penney in the XRF, EPMA and LAM–ICP–MS labs in the Department of Earth Sciences, Memorial University. Pam King carried out the wet-chemical analyses for bulk-rock $FeO/Fe_2O_3$ values. Panseok Yang is acknowledged for a conceptual version of Figure 10 and for invaluable discussions at various stages during the course of the project. The comments of the two referees, Panseok Yang and one who chose to remain anonymous, Associate Editor Dave Pattison and Robert F. Martin resulted in significant improvements to the manuscript and are gratefully acknowledged. The study was funded by Memorial University Graduate Fellowships to the first author and NSERC Discovery Grants to the second author and forms part of an ongoing investigation of the behavior of trace elements in metamorphic systems.

## References

Bea, F., Montero, P., Garuti, G. & Zaccarini, F. (1997): Pressure dependence of rare earth element distribution in amphibolite and granulite-grade garnets. A LA–ICP–MS study. *Geostandards Newsletter* **21**, 253-270.

Blundy, J.D. & Wood, B.J. (1994): Prediction of crystal–melt partition coefficients from elastic moduli. *Nature* **372**, 452-454.

Bottazzi, P., Tiepolo, M., Vannucci, R., Zanetti, A., Brumm, R., Foley, S.F. & Oberti, R. (1999): Distinct site preferences for heavy and light REE in amphibole and the prediction of $^{Amph/L}D_{REE}$. *Contrib. Mineral. Petrol.* **137**, 36-45.

Brice, J.C. (1975): Some thermodynamic aspects of the growth of strained crystals. *J. Crystal Growth* **28**, 249-253.

CARMICHAEL, D.M. (1969): On the mechanism of prograde reactions in quartz-bearing pelitic rocks. *Contrib. Mineral. Petrol.* **20**, 244-267.

CESARE, B. (1999): Multi-stage pseudomorphic replacement of garnet during polymetamorphism. 2. Algebraic analysis of mineral assemblages. *J. Metamorph. Geol.* **17**, 735-746.

DAHL, P.S., WHEN, D.C. & FELDMANN, S.G. (1993): The systematics of trace-element partitioning between coexisting muscovite and biotite in metamorphic rocks from the Black Hills, South Dakota, USA. *Geochim. Cosmochim. Acta* **57**, 2487-2505.

DEER, W.A., HOWIE, R.A. & ZUSSMAN, J. (1966): *An Introduction to the Rock-Forming Minerals*. Longmans, Green and Co., London, U.K.

ERCIT, T.S. (2002): The mess that is "allanite" *Can. Mineral.* **40**, 1411-1419.

FISHER, G.W. (1989): Matrix analysis of metamorphic mineral assemblages and reactions. *Contrib. Mineral Petrol.* **102**, 69-77.

GORDON, T.M., GHENT, E.D. & STOUT, M.Z. (1991): Algebraic analysis of the biotite–sillimanite isograd in the File Lake area, Manitoba. *Can. Mineral.* **29**, 673-686.

GRAUCH, R. (1989): Rare earth elements in metamorphic rocks. *In* Geochemistry and Mineralogy of Rare Earth Elements (B.R. Lipin & G.A. McKay, eds.). *Rev. Mineral.* **21**, 147-167.

GREEN, T.H. & PEARSON, N.J. (1986): Rare-earth element partitioning between sphene and coexisting silicate liquid at high pressure and temperature. *Chem. Geol.* **55**, 105-119.

GREENWOOD, H.J. (1967): The *N*-dimensional tie-line problem. *Geochim. Cosmochim. Acta* **31**, 465-490.

_____ (1968): Matrix methods and the phase rule in petrology. *XXIII Int. Geol. Congress* **6**, 267-279.

HARTEL, T.H.D. & PATTISON, D.R.M. (1996): Genesis of the Kapuskasing (Ontario) migmatitic mafic granulites by dehydration melting of amphibolite: the importance of quartz to reaction progress. *J. Metamorph. Geol.* **14**, 591-611.

HICKMOTT, D.D. & SHIMIZU, N. (1990): Trace element zoning in garnet from the Kwoiek area, British Columbia: disequilibrium partitioning during garnet growth? *Contrib. Mineral. Petrol.* **104**, 619-630.

_____ & SPEAR, F.S. (1992): Major and trace element zoning in garnets from calcareous pelites in the NW Shelburne Falls quadrangle, Massachusetts: garnet growth histories in retrograded rocks. *J. Petrol.* **33**, 965-1005.

JACKSON, S.E. (2001): LAMTRACE ver. 2.10: LAM–ICP–MS Data Reduction Spreadsheet for Lotus 123 ver. 5 or "MILLENIUM" for Windows 95 or NT4 Onwards. sijackso@laurel.ocs.mq.edu.au.

JAMIESON, R.A. (1979): *The St. Anthony Complex, Northwestern Newfoundland: A Petrological Study of the Relationship Between a Peridotite Sheet and its Dynamothermal Aureole*. Ph.D. thesis, Memorial Univ. of Newfoundland, St. John's, Newfoundland.

_____ (1981): Metamorphism during ophiolite emplacement – the petrology of the St. Anthony Complex. *J. Petrol.* **22**, 397-449.

_____ (1986): *P–T* paths from high temperature shear zones beneath ophiolites. *J. Metamorph. Geol.* **4**, 3-22.

_____ & STRONG, D.F. (1978): Dynamic and chemical implications of a late syntectonic shear zone within the ophiolite aureole, St. Anthony Complex, northwestern Newfoundland. *Geol. Assoc. Can. – Mineral. Assoc. Can. – Geol. Soc. Am., Abstr. Program* **3**, 428-429.

JENSEN, B.B. (1973): Patterns of trace element partitioning. *Geochim. Cosmochim. Acta* **37**, 2227-2242.

KRETZ, R. (1959): Chemical study of garnet, biotite, and hornblende from gneisses of southwestern Quebec, with emphasis on distribution of elements coexisting minerals. *J. Geol.* **67**, 371-402.

_____ (1961): Some applications of thermodynamics to coexisting minerals of variable composition. Examples: orthopyroxene–clinopyroxene and orthopyroxene–garnet. *J. Geol.* **69**, 361-387.

_____ (1983): Symbols for rock-forming minerals. *Am. Mineral.* **68**, 277-279.

_____, CAMPBELL, J.L., HOFFMAN, E.L., HARTREE, R. & TEESDALE, W.J. (1999): Approaches to equilibrium in the distribution of trace elements among the principal minerals in a high-grade metamorphic terrane. *J. Metamorph. Geol.* **17**, 41-59.

LEAKE, B.E., WOOLLEY, A.R., ARPS, C.E.S., BIRCH, W.D., GILBERT, M.C., GRICE, J.D., HAWTHORNE, F.C., KATO, A., KISCH, H.J., KRIVOVICHEV, V.G., LINTHOUT, K., LAIRD, J., MANDARINO, J.A., MARESCH, W.V., NICKEL, E.H., ROCK, N.M.S., SCHUMACHER, J.C., SMITH, D.C., STEPHENSON, N. C. N., UNGARETTI, L., WHITTAKER, E.J.W. & GUO, YOUZHI (1997): Nomenclature of amphiboles: report of the Subcommittee on Amphiboles of the International Mineralogical Association, Commission on New Minerals and Mineral Names. *Can. Mineral.* **35**, 219-246.

_____, _____, BIRCH, W.D., BURKE, E.A.J., FERRARIS, G., GRICE, J.D., HAWTHORNE, F.C., KISCH, H.J., KRIVOVICHEV, V.G., SCHUMACHER, J.C., STEPHENSON, N.C.N. & WHITTAKER, E.J.W. (2003): Nomenclature of amphiboles: additions and revisions to the International Mineralogical Association's 1997 recommendations. *Can. Mineral.* **41**, 1355-1362.

LONGERICH, H.P. (1995): Analysis of pressed pellets of geological samples using wavelength-dispersive X-ray fluorescence spectrometry. *X-ray Spectrom.* **24**,123-136.

_____, GÜNTHER, D. & JACKSON, S.E. (1996): Elemental fractionation in laser-ablation inductively-coupled mass-spectrometry. *Fresenius J. Anal. Chem.* **355**, 538-542.

MAXWELL, J.A. (1968): *Rock and Mineral Analysis*. Interscience Publishers, New York, N.Y.

MULROONEY, D. (2004): *Residence and Partitioning of REE and Selected Trace Elements in Amphibolite-Facies Metabasites: an Example from the St. Anthony Complex, Northern Newfoundland.* M.Sc. thesis, Memorial Univ. of Newfoundland, St. John's, Newfoundland.

NAGASAKI, A. & ENAMI, M. (1998): Sr-bearing zoisite and epidote in ultra-high pressure (UHP) metamorphic rocks from the Su–Lu province, eastern China: an important Sr reservoir under UHP conditions. *Am. Mineral.* **83**, 240-247.

NIELSEN, R.L. (1985): A method for the elimination of the compositional dependence of trace element distribution coefficients. *Geochim. Cosmochim. Acta* **49**, 1775-1779.

ONUMA, N., HIGUCHI, H., WAKITA, H. & NAGASAWA, H. (1968): Trace element partition between two pyroxenes and the host lava. *Earth Planet. Sci. Lett.* **5**, 47-51.

PAKTUNC, A.D. (1998): MODAN: An interactive computer program for estimating mineral quantities based on bulk composition. *Comput. Geosci.* **24**, 425-431.

PAN, YUANMING & FLEET, M.E. (1996): Intrinsic and external controls on the incorporation of rare earth elements in calc-silicate minerals. *Can. Mineral.* **34**, 147-159.

PEARCE, N.J.G., PERKINS, W.T., WESTGATE, J.A., GORTON, M.P., JACKSON, S.E., NEAL C.R. & CHENERY, S.P. (1997): A compilation of new and published major and trace element data for NIST SRM 610 and NIST SRM 612 glass reference materials. *Geostandards Newsletter* **21**, 115-144.

PYLE, J.M. & SPEAR, F.S. (1999): Yttrium zoning in garnet: coupling of major and accessory phases during metamorphic reactions. *Geological Materials Res.* **1**(6), 1-49.

_____ & _____ (2000): An empirical garnet (YAG)–xenotime thermometer. *Contrib. Mineral. Petrol.* **138**, 51-58.

SHANNON, R.D. (1976): Revised effective ionic radii and systematic studies of interatomic distances in halides and chalcogenides. *Acta Crystallogr.* **A32**, 751-767.

SKUBLOV, S. & DRUGOVA, G. (2003): Patterns of trace-element distribution in calcic amphiboles as a function of metamorphic grade. *Can. Mineral.* **41**, 383-392.

SMITH, J.V. & BROWN, W.L. (1987): *Feldspar Minerals*. 1. *Crystal Structures, Physical, Chemical, and Microtextural Properties*. Springer-Verlag, New York., N.Y.

SMYTH, J.R. & BISH, D.L. (1988): *Crystal Structures and Cation Sites of the Rock Forming Minerals*. Allen & Unwin, Boston, Massachusetts.

SORENSEN, S.S. & GROSSMAN, J.N. (1989): Enrichment of trace elements in garnet amphibolites from a paleo-subduction zone: Catalina Schist, southern California. *Geochim. Cosmochim. Acta* **53**, 3155-3177.

SPEAR, F.S. (1993): *Metamorphic Phase Equilibria and Pressure – Temperature – Time Paths*. Mineralogical Society of America, Washington, D.C.

SYLVESTER, P. (2001): Laser-Ablation – ICPMS in the Earth Sciences: Principles and Applications. *Mineral. Assoc. Can., Short Course Ser.* **29**.

TAYLOR, R.P., JACKSON, S.E., LONGERICH, H.P. & WEBSTER, J.D. (1997): In situ trace-element analysis of individual silicate melt inclusions by laser ablation microprobe–inductively coupled plasma–mass spectrometry (LAM–ICP–MS). *Geochim. Cosmochim. Acta* **61**, 2559-2567.

TAYLOR, S.R. & MCLENNAN, S.M. (1985): *The Continental Crust: its Composition and Evolution*. Blackwell Scientific, Boston, Massachusetts.

TIEPOLO, M., OBERTI, R. & VANNUCCI, R. (2002): Trace-element incorporation in titanite: constraints from experimentally determined solid/liquid partition coefficients. *Chem. Geol.* **191**, 105-119.

TRIBUZIO, R., MESSIGA, B., VANNUCCI, R. & BOTTAZZI, P. (1996): Rare earth element redistribution during high-pressure low-temperature metamorphism in ophiolitic Fe-gabbros (Liguria, north western Italy): implications for light REE mobility in subduction zones. *Geology* **24**, 711-714.

WILLIAMS, H. (1975): Structural succession, nomenclature, and interpretation of transported rocks in western Newfoundland. *Can. J. Earth Sci.* **12**, 1874-1894.

_____ (1995): Taconic allochthons in Newfoundland (Humber Zone). *In* Geology of the Appalachian–Caledonian orogen in Canada and Greenland (H. Williams, ed.). *Geol. Surv. Can.*, *Geology of Canada* **6**, 843-890 (also *Geol. Soc. Am.*, *The Geology of North America* **F–1**).

YANG, PANSEOK & RIVERS, T. (2000): Trace element partitioning between coexisting biotite and muscovite from metamorphic rocks, western Labrador: structural, compositional and thermal controls. *Geochim. Cosmochim. Acta* **64**, 1451-1472.

_____ & _____ (2001): Chromium and manganese zoning in pelitic garnet and kyanite: Spiral, overprint, and oscillatory(?) zoning patterns and the role of growth rate. *J. Metamorph. Geol.* **19**, 455-474.

_____ & _____ (2002): The origin of Mn and Y annuli in garnet and the thermal dependence of P in garnet and Y in apatite in calc-pelite and pelite, Gagnon terrane, western Labrador. *Geological Material Res.* **4**(1), 1-35.

_____, _____ & JACKSON, S. (1999): Crystal-chemical and thermal controls on trace element partitioning between coexisting garnet and biotite in metamorphic rocks from western Labrador. *Can. Mineral.* **37**, 443-468.

ZACK, T., KRONZ, A., FOLEY, S.F. & RIVERS, T. (2002): Trace element abundances in rutiles from eclogites and associated garnet mica schists. *Chem. Geol.* **184**, 97-122.

*Received October 7, 2003, revised manuscript accepted October 25, 2004.*

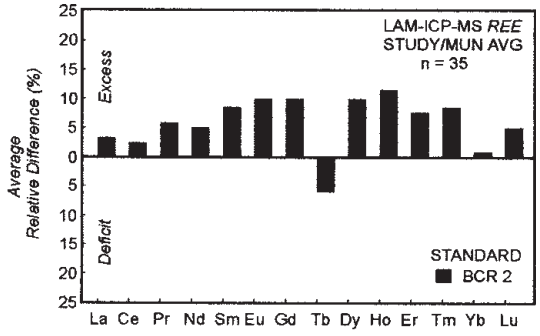


FIG. A1. Bar graph illustrating estimates of accuracy for LAM–ICP–MS analyses based on repeated measurements of standard reference material BCR–2G carried out in the course of this study, compared to the average at Memorial University of Newfoundland.

TABLE A1. ESTIMATES OF PRECISION (% RELATIVE STANDARD DEVIATION) AND ACCURACY (% DIFFERENCE) FOR LAM–ICP–MS ANALYSES USING STANDARD REFERENCE-MATERIAL BCR–2G

| BCR-2G | This study $n = 35$ | % R.S.D. | MUN average $n = 235$ | % Diff |
|---|---|---|---|---|
| La ppm | 22.16 | 5 | 24.48 | +3.24 |
| Ce | 48.90 | 4 | 52.19 | +2.62 |
| Pr | 5.93 | 4 | 6.43 | +5.89 |
| Nd | 25.25 | 3 | 27.25 | +4.83 |
| Sm | 5.54 | 9 | 6.09 | +8.72 |
| Eu | 1.73 | 5 | 1.86 | +6.93 |
| Gd | 5.37 | 7 | 6.28 | +7.71 |
| Tb | 0.80 | 32 | 1.10 | -5.65 |
| Dy | 5.33 | 6 | 5.84 | +8.54 |
| Ho | 1.02 | 10 | 1.14 | +11.49 |
| Er | 2.92 | 11 | 3.38 | +7.74 |
| Tm | 0.42 | 12 | 0.49 | +8.63 |
| Yb | 2.94 | 8 | 3.32 | +0.62 |
| Lu | 0.41 | 9 | 0.49 | +3.88 |

The 35 analyses of standard BCR–2G carried out during the course of this study were compared with the MUN average based on 235 analyses between 1996 and 2002.